

## REVIEW

# Confined nanoarchitectonics for nano-reactors: *in-situ* characterization and tracking systems at the nanoscale

Na Kong<sup>\*a</sup> and Katsuhiko Ariga<sup>\*ab</sup>Received 00th January 20xx,  
Accepted 00th January 20xx

DOI: 10.1039/x0xx00000x

Nanoscale confinement environments, such as surface-confined interfaces, porous nanostructures, nanopores, and hollow nanoparticles, are increasingly recognized as powerful platforms for controlling and enhancing chemical reactions. Confinement at the nanoscale significantly alters the physical and chemical properties of reactants, enabling novel reaction pathways, accelerated kinetics, and unique catalytic behaviours. However, constructing the required nanostructures as well as characterizing and monitoring these reactions in real-time remains a significant challenge due to the complexity of confined environments. This review provides a comprehensive overview of state-of-the-art *in-situ* characterization and tracking systems used to study reactions in confined interfaces. We explore cutting-edge techniques, including optical, electrochemical, and molecular-level monitoring approaches, which enable real-time analysis of reaction dynamics. Finally, we outline future directions for the development of more efficient *in-situ* tracking systems and advanced characterization techniques, which hold the potential to unlock new frontiers in nanotechnology and materials science.

## 1. Introduction

The real-time tracking and observation of chemical reactions has been a longstanding goal for chemists, as it is essential for achieving a complete understanding of reaction mechanisms and enabling the precise manipulation of reaction outcomes. By capturing the dynamic evolution of reactants, intermediates, and products at the molecular level, real-time monitoring provides critical insights into reaction kinetics, transition states, and the influence of external factors such as temperature, pressure, and catalysts.<sup>1, 2</sup> This capability is particularly crucial in complex reaction environments including heterogeneous catalysis and biomolecular interactions, where reaction pathways often involve multiple intermediates, competing side reactions, and transient species that are challenging to isolate and characterize using conventional methods.<sup>3</sup> In this context, nano-reactors—so-called "mini-labs"—have emerged as powerful tools for probing chemical processes under confined conditions. By restricting molecular diffusion and limiting the number of participating species, nano-reactors enable the detection and characterization of transient intermediates and rare reaction pathways that are typically obscured in bulk-phase systems.<sup>4</sup> Moreover, nanoscale confinement can significantly alter the physical and chemical properties of reactants, promoting novel reaction pathways, accelerating reaction kinetics, and enabling unique catalytic behaviours. For example, the nanoscale compartments—engineered using porous

frameworks, hollow nanostructures, micelles, and biomimetic compartments—restrict molecular motion and enhance interactions within a well-defined spatial domain.<sup>5, 6</sup> Thus, certain confined nanostructures can replicate and even surpass the functionality of natural catalytic systems, such as enzymes and organelles, by providing localized reaction environments that stabilize reactive intermediates, accelerate transformations, and prevent undesired side reactions. The ability to systematically manipulate reaction conditions within nano-reactors, coupled with real-time tracking technologies, opens new possibilities in catalysis, materials synthesis, and energy conversion, paving the way for innovative advancements in nanoscale chemistry.<sup>7</sup>

To enable the rational design and construction of confined nano-reactors, a synergistic integration of materials chemistry and analytical science is essential. Materials chemistry provides strategies for constructing well-defined spatial architectures, while analytical techniques enable detailed evaluation of their structure and function. In recent years, the concept of nanoarchitectonics has emerged as a unifying framework for the rational creation of functional nanostructures.<sup>8, 9</sup> It represents a transformative advancement beyond traditional nanotechnology, evolving from passive observation and manipulation of nanoscale materials to the active design and construction of functional architectures.<sup>10, 11</sup> While nanotechnology, which gained momentum in the late 20th century, focused on imaging and characterizing atomic and molecular structures—exemplified by breakthrough like scanning tunneling microscopy (STM)—it lacked a systematic framework for integrating these components into larger, purpose-driven systems. Nanoarchitectonics, formalized in the early 21st century by pioneers like Masakazu Aono, bridges this gap by integrating multiple disciplines—including materials

<sup>a</sup> Research Center for Materials Nanoarchitectonics, National Institute for Materials Science (NIMS), 1-1 Namiki, Tsukuba 305-0044, Japan.  
ARIGA.Katsuhiko@nims.go.jp.

<sup>b</sup> Graduate School of Frontier Sciences, The University of Tokyo, 5-1-5 Kashiwa-no-ha Kashiwa 277-8561, Japan.

chemistry, supramolecular chemistry, biotechnology, surface science, self-assembly, field-controlled organization, and advanced characterization techniques—into a cohesive design philosophy.<sup>12</sup> It provides a conceptual and practical framework for the bottom-up and hierarchical organization of atoms, molecules, and nanomaterials into higher-order functional systems with tailored properties. This framework not only accommodates but actively exploits stochastic phenomena such as thermal fluctuations, quantum effects, and non-equilibrium conditions, which are often considered limitations in classical engineering paradigms.<sup>13, 14</sup> By doing so, nanoarchitectonics serves as a foundational strategy for the rational construction of confined nano-reactors that are well-suited for integration with characterization methods.

In materials chemistry, a variety of techniques have been employed to construct nanostructured materials with controlled geometries. These include self-assembly<sup>15, 16</sup> and related organization,<sup>17, 18</sup> subsequent materials conversion processes,<sup>19, 20</sup> the Langmuir-Blodgett (LB) method<sup>21, 22</sup> and layer-by-layer (LbL) assembly.<sup>23, 24</sup> Particularly noteworthy are metal-organic frameworks (MOFs)<sup>25, 26</sup> and covalent organic frameworks (COFs),<sup>27, 28</sup> which are highly effective in constructing well-ordered and tunable nanospaces due to their modular architectures and inherent porosity. These crystalline frameworks are composed of organic linkers and metal ions (in the case of MOFs) or covalent bonds (in COFs), enabling the formation of periodic, uniform pore structures with precise spatial control at the molecular level. Such features make them ideal candidates for confined reaction environments, where spatial confinement, molecular selectivity, and diffusion control are critical for optimizing reaction kinetics and pathways. Applications of the nanoarchitectonics framework have rapidly expanded across diverse fields, from fundamental sciences,<sup>29, 30</sup> to energy storage and conversion,<sup>31, 32</sup> environmental remediation,<sup>33, 34</sup> and biomedical engineering.<sup>35, 36</sup> Notably, the design of nano-reactors—where precise structural control and functional diversity are paramount—stands to benefit significantly from the nanoarchitectonics approach. Given its central relevance, this review focuses on exploring the principles, strategies, and applications of nanoarchitectonics in the context of confined nano-reactor systems.

To fully realize the potential of nano-reactors, advanced *in-situ* characterization and tracking methods are essential. The ability to observe and analyse confined reactions in real time requires state-of-the-art analytical techniques such as high-resolution transmission electron microscopy (HRTEM), scanning tunneling microscopy (STM), X-ray absorption spectroscopy (XAS), and tip-enhanced Raman spectroscopy (TERS). These tools allow researchers to visualize structural and chemical transformations at the atomic and molecular levels, offering new insights into the dynamics of reactions occurring within nanoscale confinement. In parallel, the integration of computational modelling with experimental observations has proven to be a powerful tool to elucidate reaction mechanisms, predict molecular behaviour under confinement, and guide the rational design of nano-reactors. The synergy between theory and experiment help researchers to develop predictive models

that correlate structural parameters with functional performance, thereby accelerating the optimization of nanoconfined systems.

Recent frontier reviews<sup>37–41</sup> have extensively summarized the unique chemical and physical behaviours of molecules under nanoconfinement, highlighting that confinement can profoundly influence their properties. For instance, Grommet and colleagues<sup>37</sup> have systematically categorized the diverse effects of confinement on chemical reactivity in synthetic systems, showing that nanoscale environments can enhance reaction rates, improve product selectivity, and stabilize transient intermediates. Additionally, nanoconfinement also affects physical phenomena such as fluorescence emission, optical absorption of dyes, and electronic interactions between redox-active species, all of which can be finely tuned by engineering the geometry and chemical nature of the confined space. Within these categories, researchers have developed design principles and strategies that are broadly applicable across various confined systems. Ma et al.<sup>41</sup> have recently defined the fundamental structural characteristics of porous nano-reactors, while also exploring their design principles and synthetic chemistry in the context of emerging applications in energy storage and heterogeneous catalysis.

This review aims to explore the latest advancements in confined nanoarchitectonics for nano-reactors, emphasizing the application of nanoarchitectonic principles to design more efficient and functional systems. We also emphasize the integration of *in-situ* characterization and tracking methodologies at the nanoscale, which are crucial for monitoring and understanding reactions in confined environments. By exploring the fundamental principles underlying nanoconfinement effects, the various types of nano-reactors, and cutting-edge techniques for probing confined reactions, this review provides a comprehensive overview of the field. Furthermore, we discuss the key challenges facing the development of nano-reactors and outline future opportunities for advancing their design and expanding their applications in diverse scientific and industrial domains.

## 2. Confined structure of nano-reactors

### 2.1 Dimensionality of confinement in nano-reactors

Within various nano-reactors, the confined nanostructure plays a pivotal role in determining the behaviour of reacting species, as it directly influences their degrees of freedom and interaction dynamics with the surrounding environment. From the geometric view, the confined space can be classified by dimensionality (zero-, one-, two-, and three-dimensional), which imposes distinct spatial constraints on molecular motion as illustrated in Figure 1. The degree of confinement increases as the dimensionality decreases, meaning that lower-dimensional systems impose greater spatial restrictions on molecular motion and interactions.<sup>42</sup> This high confinement regime is particularly advantageous for reactions requiring precise molecular alignment or stabilization of reactive intermediates, as the restricted spatial environment can

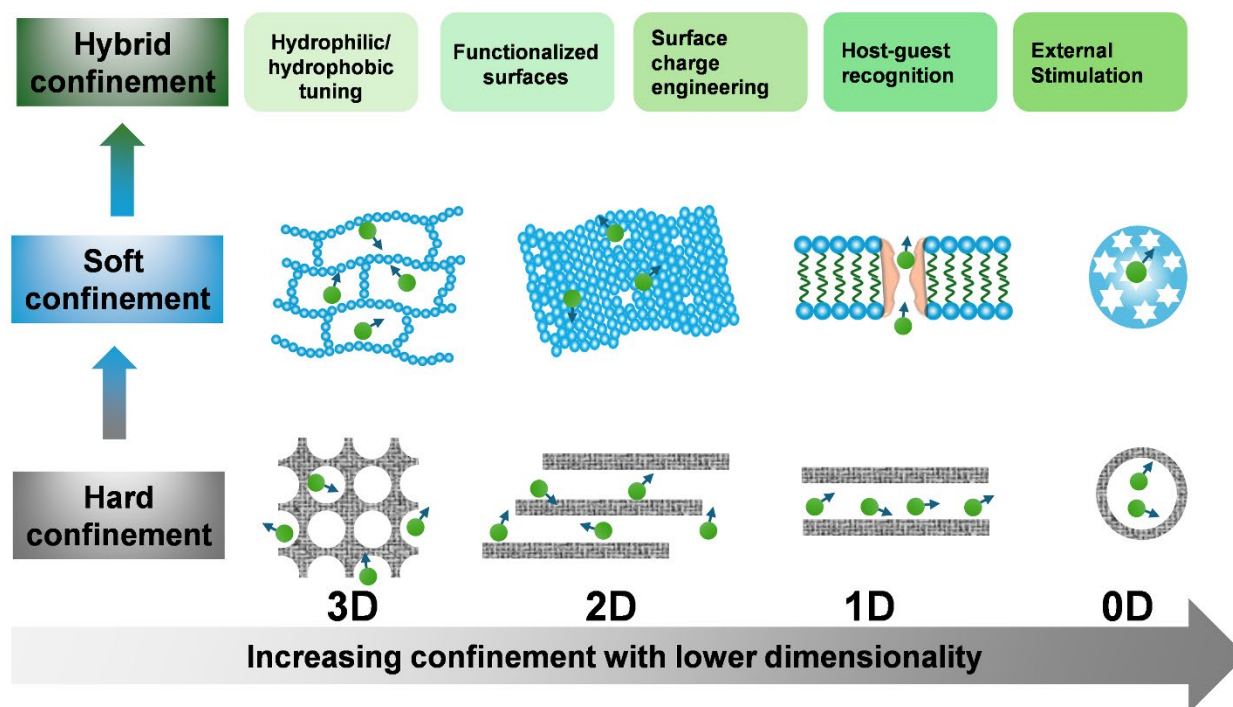


Fig. 1. Typical confined nanostructures are classified into zero-dimensional (0D), one-dimensional (1D), two-dimensional (2D), and three-dimensional (3D) architectures based on the degree of geometric and dimensional freedom available to reactants within the confined environment. These nanostructures can be further categorized into hard, soft, and hybrid confinement based on the nature of the confining medium and its interaction with the reactants. Green balls and arrows represent the reactants and their reaction directions, respectively, providing a visual understanding of the dynamic processes occurring within these confined systems.

enforce specific molecular orientations, reduce conformational flexibility, and enhance the local concentration of reactants.<sup>39, 43, 44</sup> These effects collectively contribute to improved reaction selectivity, suppressed side reactions, and the stabilization of short-lived transition states or radical species that would otherwise rapidly decompose in bulk solution.

In zero-dimensional (0D) confinement, where molecules are trapped within discrete nanocavities<sup>44, 45</sup> or molecular cages,<sup>46, 47</sup> reactants experience the highest level of confinement, significantly restricting diffusion and enhancing molecular interactions. In one-dimensional (1D) confinement, molecules are restricted within narrow channels or tubular structures, such as carbon nanotubes or mesoporous silica, allowing movement only along a single axis.<sup>48, 49</sup> This level of confinement still imposes strong diffusion constraints but provides a controlled pathway for molecular transport, leading to enhanced selectivity in catalytic and separation processes. Two-dimensional (2D) confinement,<sup>50</sup> as seen in layered materials like graphene oxide,<sup>51</sup> metal oxides,<sup>50</sup> and MXenes,<sup>52, 53</sup> allows movement along a plane while restricting access in the perpendicular direction. This type of confinement enables unique interfacial interactions and tunable reaction environments, making it highly valuable in electrochemical applications, catalysis, and energy storage. In contrast, three-dimensional (3D) confinement, observed in porous frameworks like MOFs,<sup>54, 55</sup> COFs,<sup>56</sup> and zeolites,<sup>57</sup> provides a more open environment with interconnected pores that allow reactants to diffuse in multiple directions. Unlike lower-dimensional confinement, which restricts movement along one or two axes, 3D confinement offers a balance between spatial restriction and

accessibility, facilitating complex interactions and efficient mass transport. The interconnected nature of these 3D frameworks not only enhances reactant mobility but also enables synergistic effects, such as cooperative catalysis or multi-step reactions, which are difficult to achieve in lower-dimensional systems. The spatial constraints imposed by the walls or matrices of nano-reactors restrict the movement and orientation of molecules, ions, or nanoparticles, resulting in altered physical, chemical, and mechanical properties. Thus, a large number of opportunities could be realized by producing dimensionality-controlled nanostructures in the reaction/reactants comfortable confinement regime, which could lead to the success of potential applications.<sup>58</sup>

## 2.2 Soft vs. hard confinement: structural and dynamic effects

Although the geometric classification of confined nanostructure provides a foundational understanding of spatial constraints, the structural rigidity, dynamic adaptability, and interaction mechanisms within the confined space also play a crucial role in dictating reaction kinetics, molecular transport, and selectivity within nano-reactors. The confinement can further be categorized into soft confinement and hard confinement which provides a fundamental framework for understanding how different nanoarchitectures influence reaction environments at the nanoscale. Hard confinement, typically associated with rigid materials like inorganic porous frameworks or carbon nanotubes, imposes fixed spatial restrictions on reactants.<sup>59</sup> Due to their rigid frameworks, these materials possess ordered pore structures with uniform dimensions, which enable selective adsorption, diffusion, and reaction of molecules based on their size, shape, and chemical properties. MOFs are a

prominent example of hard confinement, consisting of metal ions or clusters coordinated to organic ligands to form crystalline, porous structures.<sup>5</sup> The high surface area and tunable pore sizes of MOFs make them ideal for applications such as gas storage, separation, and catalysis. For instance, the confinement of reactants within the pores of a MOF can enhance reaction selectivity by restricting the orientation and movement of molecules, thereby favouring specific reaction pathways.<sup>60</sup>

In contrast, soft confinement refers to nano-reactors that are flexible, dynamic and capable of undergoing structural changes in response to external stimuli.<sup>61</sup> The structural integrity of these systems is typically maintained through weak, non-covalent interactions such as hydrogen bonding, electrostatic forces, and van der Waals interactions, which allow for reversible and responsive control over molecular interactions and reaction pathways.<sup>62, 63</sup> Examples of soft confinement include micelles, vesicles, supramolecular gels, liquid crystals, and functionalized interfaces.<sup>64–66</sup> Soft confinement offers the advantage of adaptability and stimuli-responsiveness, making it suitable for dynamic systems where environmental conditions may vary. For example, in drug delivery systems, soft-confined carriers such as liposomes can release their payload in response to specific triggers, such as changes in pH or temperature, ensuring targeted and controlled drug delivery.<sup>67</sup> However, its structural flexibility can sometimes lead to lower mechanical stability and reproducibility compared to hard confinement systems. On the other hand, while hard confinement excels in providing well-defined reaction environments, it often lacks tunability and adaptability, making it less suitable for processes requiring real-time environmental responsiveness.<sup>68</sup> By combining the advantages of soft and hard confinement, researchers can design hybrid systems that exhibit both adaptability and precision.

Surface and structural engineering through the nanoarchitectonics approach highlights the potential of synergistically leveraging the complementary properties of soft and hard confinement to design multifunctional nano-reactors for advanced applications. By integrating these confinement strategies, researchers can precisely tailor reaction environments at the nanoscale, optimizing parameters such as mass transport, reactant accessibility, and localized microenvironmental conditions (e.g., pH, polarity, and mechanical stress). For example, hydrophilic/hydrophobic tuning enables the selective partitioning of reactants based on their polarity, while functionalized surfaces and surface charge engineering can enhance substrate binding and orientation, improving catalytic efficiency. Host-guest recognition mechanisms, such as the selective binding of specific molecules within MOF cavities, further refine reaction specificity. Additionally, external stimulation—such as light, temperature, or magnetic fields—can dynamically modulate the properties of soft materials, enabling real-time control over catalytic activity or molecular release. Still taking MOFs as an example, a burgeoning field focuses on encapsulating soft functional materials—such as polymers, biomolecules, or ionic liquids—within the pores, matrices, or interlayers of MOFs, or

alternatively, encapsulating/coating MOFs with soft supports like hydrogels, polymers, or lipid bilayers.<sup>69, 70</sup> These hybrid architectures demonstrated enhanced catalytic activity, selectivity, and stability due to the synergistic interplay between the dynamic adaptability of soft materials and the structural rigidity of MOFs.

### 3. Nanoarchitectonics for nano-reactors

The primary benefit of nanoarchitectonics<sup>71–73</sup> lies in its ability to precisely control the spatial arrangement and functional integration of materials unit—ranging from atoms, molecules to complex nanomaterial—by combining insights from nanotechnology, materials science, and other interdisciplinary fields. In this section, we will focus on the design and construction of nano-reactors with highly tailored architectures, specifically those with specific functionalities that influence reaction pathway and dynamics. It also explores the integration of multi-functional components to achieve synergistic effects that enhance overall reactor performance.

#### 3.1 Reduce reaction volume/confine the reaction space

Nanoarchitectonics offers a transformative approach for designing single-molecule nano-reactors by creating environments that match the dimensions of individual molecules or particles, typical in 0D and 1D nanostructures. These precisely tailored spaces allow single entities to be captured, confined, and manipulated with exceptional control, providing unprecedented insights into their behaviour and reactivity.<sup>74, 75</sup> Such systems include caged molecules,<sup>13</sup> supramolecular assembled spaces,<sup>76, 77</sup> natural nanopores/nanochannels,<sup>2, 78</sup> plasmonic nanocavities,<sup>79</sup> and micro-nano fabricated junctions,<sup>80–84</sup> enable researchers to investigate how single-molecule or single-particle processes differ from bulk reactions, uncovering fundamental mechanisms that are often masked in larger-scale systems. Table 1 gives some examples of investigating single molecule dynamics that confined within nanospace.

The construction of molecular spaces with precise structure relies heavily on the principles of molecular recognition which is driven by non-covalent interactions such as hydrogen bonding,  $\pi$ - $\pi$  stacking, and electrostatic forces. These interactions facilitate the selective and directional assembly of molecules into highly ordered architectures. Supramolecular complexes, such as molecular peapods formed by carbon nanotubes encapsulating fullerenes, exemplify the power of non-covalent interactions in creating confined molecular spaces.<sup>85, 86</sup> In these systems, fullerenes are trapped within the cylindrical cavities of carbon nanotubes, forming an annular closed space that can incorporate additional guest molecules. The assembly of these supramolecular complexes is governed by weak intermolecular interactions, including van der Waals forces and CH- $\pi$  hydrogen bonds. The combination of multiple synergistic interactions results in remarkably high aggregation constants in solution, stabilizing the complexes despite the weak nature of individual interactions.<sup>87</sup>

Table 1 Confined nanostructure for single molecule study.

Confined structure	Characterization	Acquired information	Refs.
Graphene single-molecule junction	Real-time measurement of currents	Detection of reactive intermediates; quantitative analysis of reaction kinetics/dynamics	80
Water molecule anchored in the C60 fullerene	Scanning tunneling microscope-based break junction	Water molecules free from any hydrogen-bonding	13
Nanopore	Real-time electrical trajectory	DNA/RNA sequence; molecule interaction dynamics	2, 78
Plasmonic nanocavity	Single-molecule Raman scattering spectroscopy	Vibrational signatures of chemical bonds; identify reaction intermediates and reveal underlying reaction mechanisms;	79
Porous hollow SiO <sub>2</sub> nanosphere confined redox molecule	Single-molecule fluorescence microscopy	Molecular reaction kinetics and dynamics of elementary reactions	77
Probe-sample junction	Quantum tunneling phenomenon through scanning tunneling microscopy	Molecular surface electronic structures, molecular orbitals and local electron density states	81, 83
Probe-sample junction	Weak interaction forces by atomic force microscopy	Topological structure, morphology and physical properties of molecules on the substrate surface	82, 84
Porous zeolite-confined single molecules	Scanning transmission electron microscopy	Adsorption and desorption behaviours; molecular interaction; single molecule imaging	88, 89

In nanoporous structures, each pore can serve as an individual reaction site, enabling precise control over chemical processes. These porous structure such as MOF<sup>54, 60</sup> and zeolites,<sup>88, 89</sup> can be multifunctionally engineered by strategically incorporating catalysts and modulators within the pores to enhance both reactivity and selectivity. For instance, an enantiopure prolinyl group was introduced into the cavity of a MOF as a catalytic site for asymmetric aldol reactions.<sup>90</sup> Opposite the catalytic site, a 'selectivity modulator' was installed to provide steric hindrance, which significantly increased the enantiomeric excess of the reaction. Additionally, a series of alkyl groups were covalently attached within the pore to act as 'reactivity modulators,' fine-tuning the overall reaction yield. This approach demonstrates how the spatial organization of functional groups within a confined environment can be leveraged to optimize catalytic performance.

Furthermore, the nanoarchitectonics concept emphasizes the integration of multiple levels of organization, from the molecular scale to the macroscopic scale. A compelling example of this approach is the synthesis of mesoporous graphitic carbon nitride (g-C<sub>3</sub>N<sub>4</sub>) nanorods (NRs) through a nano-confined thermal condensation process.<sup>91</sup> In this method, cyanamide is thermally condensed within silica nanotubes (NTs) featuring porous shells. The confined environment of the silica NTs, combined with the retention of gas bubbles during condensation and the limited availability of the cyanamide precursor, facilitates the formation of mesoporous g-C<sub>3</sub>N<sub>4</sub>. This nano-confined synthesis represents a significant advancement over traditional templating methods, as it enables precise control over the material's porosity and morphology without the need for additional templating agents. The resulting mesoporous g-C<sub>3</sub>N<sub>4</sub> NRs exhibit exceptional photocatalytic properties, including remarkably enhanced activity and stability in applications such as water splitting and the degradation of organic pollutants like Rhodamine B. The interconnected mesopores facilitate the diffusion of reactants and products, while the nanorod morphology enhances light harvesting and electron transport. These properties make mesoporous g-C<sub>3</sub>N<sub>4</sub>

NRs highly promising for sustainable energy and environmental remediation applications.

### 3.2 Increase the active reaction sites

Unlike downsizing nano-reactors to the single-molecule scale, which often limits the accessibility of active sites and restricts mass transport, 2D and 3D nanostructures offer abundant accessible surface sites for catalysing reactions or immobilization of reactive centres. Their high surface areas, tailored porosity, and hierarchical architectures significantly improve catalytic performance by optimizing reactant diffusion, active site exposure, and structural stability.

Among various electrocatalytic oxidation catalysts, which require a highly exposed electrochemically active area and an optimal electron transfer structure, layered double hydroxides (LDHs), particularly NiFe-LDH, have emerged as promising candidates in alkaline solutions.<sup>50</sup> However, their oxygen evolution reaction (OER) performance is often hindered by poor electronic conductivity and a limited number of active sites. To address these challenges, Tang and co-workers<sup>92</sup> employed a surface-confined synthesis strategy to fabricate a composite of nanometer-sized NiFe-LDHs (NiFe-LDHs) on a porous nitrogen-doped graphene framework (NGF). The nitrogen dopants and topology-induced defects in the NGF provided abundant adsorption sites for the uniform growth of NiFe-LDHs. The resulting NiFe-LDHs exhibited exceptional OER performance under alkaline conditions. The enhanced OER activity was attributed to the unique structural features of this hierarchical composite: (1) the mesoporous NGF scaffold provided high conductive and facilitated efficient electron transfer; (2) the dispersed NiFe-LDHs introduced numerous active species while modifying surface properties; and (3) the doping nitrogen tailored the electronic structure of the hybrid material, further boosting catalytic activity. The OER performance of NiFe-LDH can be further improved by decorating single gold (Au) atoms on the LDH surface through a surface-confined synthesis strategy.<sup>93</sup> As shown in Figure 2a, the resulting single Au/NiFe-LDH catalyst exhibited a sixfold enhancement in OER activity



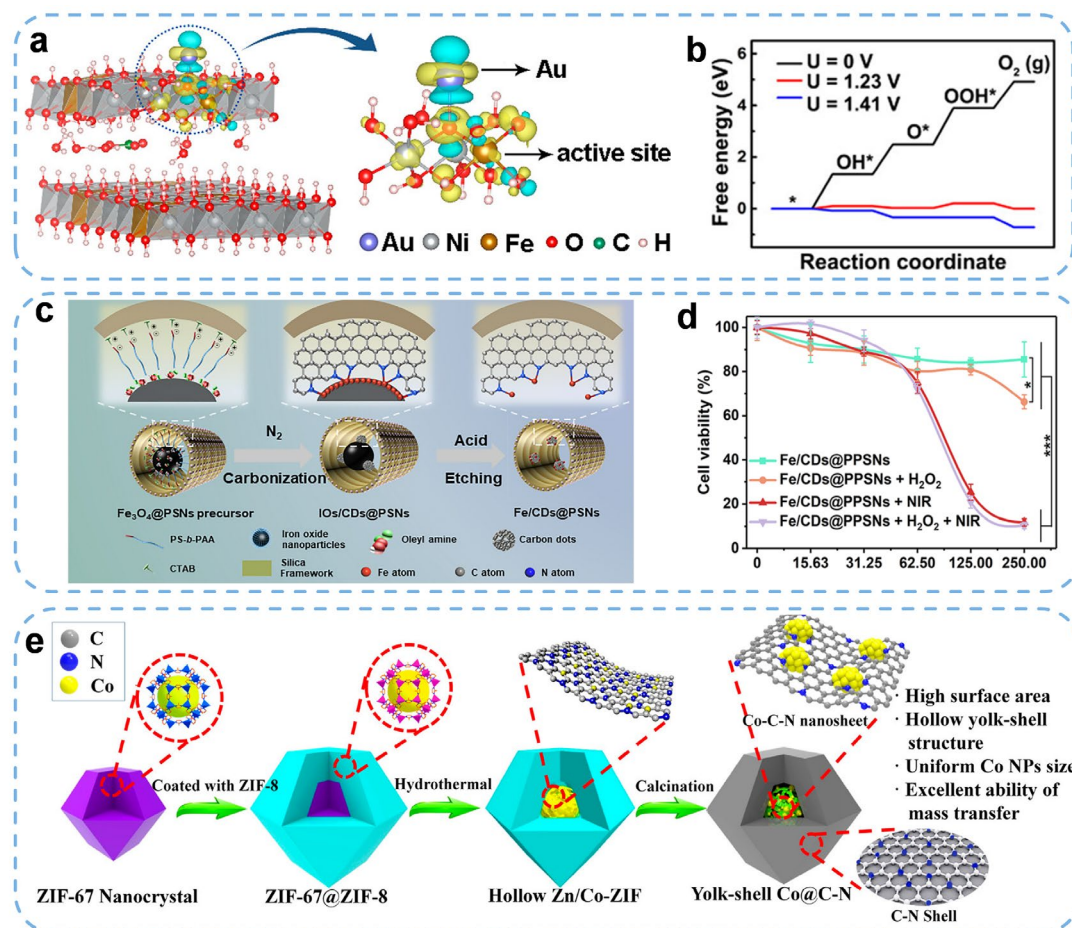


Fig. 2 (a) Differential charge densities of NiFe LDH with and without Au atom when one O atom is adsorbed on the Fe site. Iso-surface value is 0.004 eÅ<sup>-3</sup>. Yellow and blue contours represent electron accumulation and depletion, respectively. (b) Free energy diagram for the OER at different potentials on the surface of sAu/NiFe LDH model. Copyright 2018, American Chemical Society. (c) Schematic illustration for the synthesis and biological effect of Fe/CDs@PPSNs. (d) The therapeutic effect of Fe/CDs@PPSNs against tumor cells. Copyright 2022, Nature Publishers. (e) Schematic illustration of the synthesis of hollow yolk-shell Co@C-N nano-reactors. Copyright 2018, American Chemical Society.

compared to pristine NiFe-LDH, achieving an overpotential of just 237 mV at a current density of 10 mA cm<sup>-2</sup>. This enhancement is further supported by density functional theory (DFT) calculations of the free energy changes associated with key OER intermediates (OH\*, O\*, and OOH\*), as presented in Figure 2b. The observed decrease in overpotential is attributed to the role of single Au atoms to induce charge redistribution around the active Fe centers and adjacent atoms, thereby modulating the local electronic environment and facilitating more favourable reaction kinetics.

From the structural evolution perspective, 3D hollow nanostructures can be regarded as spatially curved and enclosed derivatives of 2D nanosheets. These architectures combine the high reactivity of 2D nanomaterials with the mechanical robustness and diffusion advantages of 3D frameworks.<sup>94</sup> The self-supported nature imparts enhanced structural stability, minimizing aggregation and degradation of active centres during catalytic processes. Additionally, their high surface-to-volume ratio offers a rich density of unsaturated coordination sites. The discrete voids within these nanostructures serve dual purposes: they trap metastable reaction intermediates at reactive sites for further transformation and concentrate reactants through selective

interactions. The uniform channel and pore structures in these materials further facilitate efficient mass transfer and molecular sieving. A notable demonstration of such advanced design is provided by Qin et al. al.,<sup>95</sup> who employed an interfacial-confined coordination strategy to construct iron single-atom-anchored defective carbon dots within PEGylated porous silica nano-reactors (Fe/CDs@PPSNs, as illustrated in Fig. 2c). This approach involved the *in-situ* high-temperature carbonization of polymers precursors, leading to the formation of nitrogen-doped carbon dots. During this process, interfacial coordination between nitrogen atoms and iron atoms occurred, stabilizing them at atomic precision. Subsequent acid etching selectively removed excess iron-based nanoparticles, resulting in a biocompatible, chemically stable nano-reactor featuring single-atom Fe-N-C active sites. Under near-infrared (NIR) irradiation, the material exhibited a tumor-specific therapeutic effect and an excellent photothermal response (Fig. 2d), attributed to the Fe single-atom-anchored defective carbon framework. This unique combination of properties highlights the potential of such nanostructures in advanced catalytic applications, particularly in biomedicine and environmental remediation. Another promising strategy involves the incorporation of nanoparticles, organic ligands, and other functional units to

construct novel architectures that increase the density of active reaction sites. Among these, hollow yolk-shell nanostructures have garnered significant attention due to their unique core-shell architecture.<sup>96</sup> The interstitial void space between the shell and core in such systems provides a confined reaction chamber that concentrates reactants and stabilizes intermediates. As illustrated in Fig. 2e, a yolk-shell Co@C–N nano-reactor<sup>97</sup> was synthesised to prevent cobalt (Co) aggregation via the thermolysis of a hollow Zn/Co-ZIF precursor. The thickness of the C–N shell and the size of the Co nanoparticles (NPs) could be precisely controlled by adjusting preparation parameters, such as crystallization time and calcination temperature. The C–N nanosheets lining the internal cavity were found to play a dual role: they effectively stabilized the Co NPs and facilitated electronic synergistic effects via synergistic interactions. Additionally, the confined hollow cavity and porous C–N shell promoted efficient mass transport while preventing the leaching of Co NPs during reactions. The integration of advanced building units, sophisticated synthesis techniques, and theoretical insights has significantly accelerated the discovery and optimization of nanostructures for specific catalytic applications. Through a combination of experimental approaches and computational modelling, researchers can now design materials with optimized electronic configurations, structural stability, and catalytic efficiency, paving the way for high-performance, application-specific nano-reactors.<sup>98</sup>

### 3.3 Confine the reaction boundary

A key application of nanoscale confinement is the regulation of reaction dimensionality and molecular assembly. By restricting reactants within anisotropic nanoscale environments—such as nanotubes, nanochannels, or layered architectures—researchers can precisely manipulate reaction pathways, crystallization processes, and resulting material properties.<sup>99, 100</sup> Strategies involving nanotemplates—such as anodic aluminum oxide (AAO) membranes, mesoporous silica, or block copolymers—provide predefined nanochannels or cavities that physically confine reactants, guiding the formation of nanowires, nanotubes, or quantum dots with uniform sizes and morphologies.<sup>101, 102</sup> For instance, AAO templates have been widely used to fabricate highly ordered metal or semiconductor nanowire arrays via electrochemical deposition, offering tunable diameter and length based on pore dimensions. Similarly, self-assembled monolayers (SAMs), composed of molecules like alkanethiols or silanes on metallic or oxide surfaces, create chemically functionalized surfaces that direct molecular orientation and assembly.<sup>103, 104</sup> In nanopatterned SAMs, specific functional groups can attract or repel reactants, enabling site-selective reactions, nanoparticle deposition, or molecular imprinting. This precise molecular arrangement is crucial for fabricating devices such as organic field-effect transistors (OFETs), biosensors, and nanopatterned catalysts, where spatial precision at the nanoscale directly influences device performance.<sup>105</sup>

In the context of solid-state synthesis, Tokmachev et al.<sup>106</sup> explored how reaction dimensionality influence material

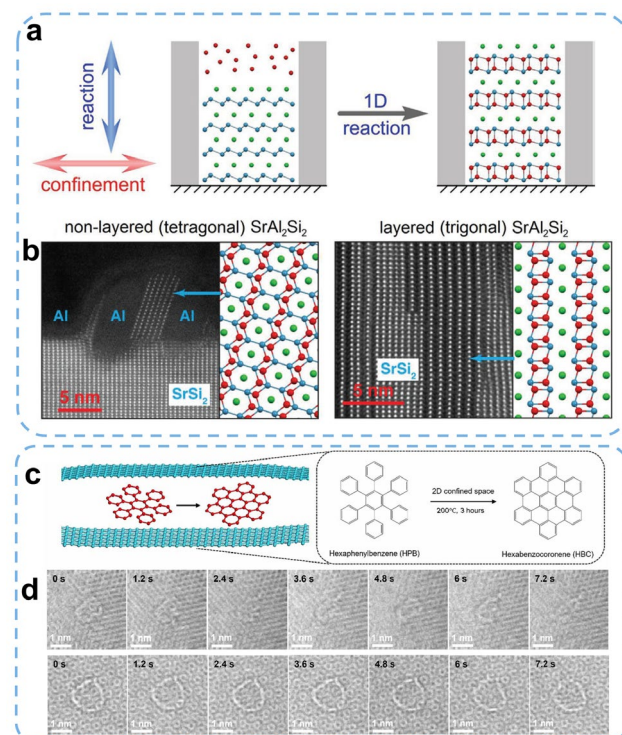


Fig. 3 (a) Mutual orientation of reaction and confinement directions in 1D reactions. (b) High-angle annular dark-field STEM images of formed non-layered (tetragonal)  $\text{SrAl}_2\text{Si}_2$  and layered (trigonal)  $\text{SrAl}_2\text{Si}_2$  structure. Copyright 2023, Wiley VCH. (c) Cyclodehydrogenation reaction of HPB between layers of graphene or hBN. Schematic illustration of cyclodehydrogenation of HPB confined between graphene layers. (d) Sequential images of HPB (Top) and HBC (Bottom) confined in the graphene sandwich. Copyright 2024, AAAS.

formation, using 1D synthesis as a case study (Fig. 3a). Their work highlighted the importance of directional confinement—whether align parallel or orthogonal to the reaction direction—in determining reaction outcomes. Using molecular beam epitaxy, they synthesized and characterized layered and non-layered compounds, demonstrating that geometric constraints can steer material growth by modulating interfacial interactions and mass transport (Fig. 3b). Directional confinement thus provides an additional level of control over material composition, morphology, and ultimately, physical properties. These findings underscore the potential of nanoscale confinement as a versatile tool for tailoring material properties, including catalytic activity, electronic behaviour, and mechanical strength.

Two-dimensional (2D) nanostructured confinement provides a fascinating and highly controlled environment for dimensional confinement synthesis. The unique properties of 2D materials, such as graphene and hexagonal boron nitride (h-BN), enable the creation of atomically thin spaces where reactants experience extreme pressures—up to 7 GPa—and highly restricted geometries.<sup>107</sup> These conditions facilitate chemical reactions that are otherwise unattainable under standard conditions, such as solvent-free organic transformations and catalytic processes. As shown in Fig. 3c,<sup>108</sup> the cyclodehydrogenation of hexaphenylbenzene (HPB) to form hexabenzocoronene (HBC), a reaction that typically requires catalysts, can proceed spontaneously under the high-pressure

conditions created by graphene confinement. In this experiment, graphene/HPB/graphene (G/HPB/G) pressure vessels were subjected to thermal annealing, which induced strong coupling between graphene layers and produced a well-defined confined van der Waals pressure within the sandwich structure. Remarkably, the formation of HBC from HPB to HBC was confirmed by high-resolution transmission electron microscopy (Fig. 3d), underscoring the critical role of interfacial confinement and layer coupling in facilitating this reaction, even under milder thermal conditions. Similarly, the oxidative polymerization of dopamine into sheet-like crystalline structures was also achieved using this approach. These findings highlight the power of 2D-confined systems to perform high-pressure chemistry without the need for external mechanical compression, offering a scalable and energy-efficient pathway to novel material synthesis.

### 3.4 Changing the active species distribution

The active species in a chemical reaction include reactants, catalysts, intermediates, and final products. The spatial distribution of these species within nano-reactors plays a critical role in determining reaction pathways, kinetics, and product yields. Nanoarchitectonics has proven effective in designing structured environments where active species are precisely arranged to optimize interactions, enhance catalytic performance, accelerate reaction kinetics, and facilitate *in-situ* product separation, ultimately enabling more sustainable and efficient chemical processes.

One of the fundamental strategies in nanoarchitectonics is the precise loading and arrangement of catalysts within confined spaces. This approach enhances the accessibility of active sites and improves the overall efficiency of catalytic processes. For instance, Prieto et al.<sup>109, 110</sup> reported the real-time observation of water formation by confining O and H<sub>2</sub> on a Ru(0001) surface covered with a vitreous SiO<sub>2</sub> bilayer (Fig. 4a and b). The SiO<sub>2</sub> bilayer, interacting with the Ru(0001) substrate via van der Waals forces, created a confined space where molecules could intercalate. At the atomic scale, the SiO<sub>2</sub> framework consists of corner-sharing SiO<sub>4</sub> tetrahedral units, forming ring-like structures that define channels for molecular diffusion. Microkinetic modelling revealed that H<sub>2</sub> molecules dissociated almost anywhere in the O-poor region, while water formation occurred predominantly near the reaction front due to the concentration gradient in adsorbed oxygen species (O<sub>ads</sub>). This study highlights the critical influence of spatial confinement and species distribution on reaction kinetics. To further exemplifying this principle, Wang et al.<sup>111</sup> constructed a Fe–Co dual-site catalyst embedded in N-doped carbon nanotubes (CNTs) by precisely controlling the bonding between Fe<sup>3+</sup> precursors and Co nodes of Zn/Co bimetallic metal–organic frameworks (BMOFs). Experimental and DFT results demonstrated that the Fe–Co dual sites effectively weakened the O=O bonds, thereby promoting oxygen activation. This work illustrates how nanoarchitectonics can be used to design catalysts with tailored active sites to achieve more efficient and selective reactions. Related dual metal sites catalysts,<sup>112</sup> including dual-atom catalysts<sup>113, 114</sup> could also be extended to

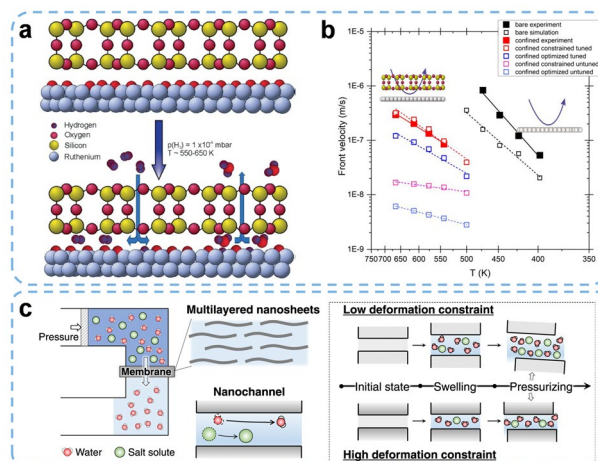


Fig. 4 (a) The water formation reaction in the confined space under a vitreous SiO<sub>2</sub> bilayer supported on Ru (0001). Copyright 2018, Wiley VCH. (b) Experimental and theoretically derived Arrhenius plots of the reaction front velocity as a function of temperature obtained for the nonconfined and confined reactions and uncovered Ru(0001). Copyright 2022, American Chemical Society. (c) Illustrations of reverse osmosis system, multilayered nanosheet membrane, and interlayered nanochannels. Copyright 2023, Nature Publishers.

other nanostructures such as 2D graphene and 3D porous MOFs in heterogeneous catalysis.

The ability to separate products *in-situ* is another critical advantage of nanoarchitectonics, as it prevents catalyst poisoning and ensures continuous reaction cycles. This is particularly important in biomass conversion, where the presence of alkali, alkaline-earth (e.g., K, Na, Mg, Ca), and transition metals (e.g., Fe, Cu) can poison catalysts by deactivating acidic or hydrogenation sites.<sup>115</sup> To address these challenges, strategies such as developing contaminant-tolerant catalysts or selecting appropriate supports can promote the desorption of nonmetal contaminants from active sites, thereby maintaining catalytic activity and enhancing process efficiency. The zeolite framework like ZSM-5 has demonstrated relative ion-exchange selectivity, where metal ions with larger radii exhibit higher ion-exchange selectivity.<sup>116</sup> Additionally, monovalent ions are often more easily exchanged into the zeolite compared to polyvalent ions. As a result, such porous zeolites hold great potential as catalytic supports for industrial applications. For the hydrogenation of C=O/C–O bonds, a high partial pressure of H<sub>2</sub> is crucial to obtain favourable conversion and selectivity. However, under such conditions, unwanted over-hydrogenation becomes a concern. Morphological control through core–shell architectures offers a solution by isolating active sites and enabling stepwise transformation of intermediates. In the hydrogenation of dimethyl oxalate (DMO), a copper silicate nano-reactor with a nanotube-assembled hollow sphere (NAHS)<sup>117</sup> exhibited exceptional catalytic performance. This system achieved a 95% yield of ethylene glycol and maintaining stability for over 300 hours, even at a low H<sub>2</sub>/DMO molar ratio of 20 (compared to the typical range of 80–200). Comparative studies with nanotube and lamellar-shaped Cu/SiO<sub>2</sub> catalysts revealed that the concave surfaces of the nanotubes and hollow spheres enhanced hydrogen enrichment, thereby boosting catalytic activity. Additionally, the spatial



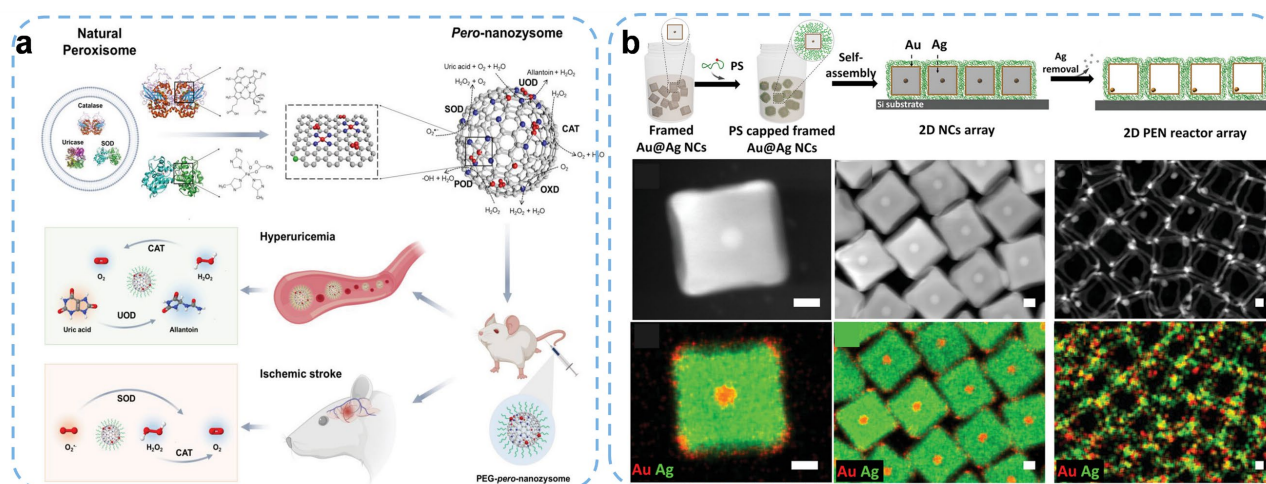


Fig. 5 (a) Schematic illustration of designing artificial peroxisome using nanozyme (pero-nanozyme) with iron doping for ameliorating hyperuricemia and ischemic stroke. Copyright 2020, Wiley VCH. (b) Fabrication and characterization of cell sheet-like soft PEN reactor arrays. up) Schematic diagrams of the framed core-shell Au@Ag NC suspension before and after PS modification and schematic diagrams of a self-assembled 2D framed Au@Ag NC array and a PEN reactor array. v–vi) HAADF-STEM images of an Au@Ag NC, 2D framed Au@Ag NC array, and PEN reactor array. Copyright 2021, Wiley VCH.

confinement effect within the NAHS structure allowed for precise control over selectivity and product distribution. By adjusting the length of the nanotubes on the NAHS, researchers could fine-tune the yields of methyl glycolate and ethylene glycol, highlighting the potential of morphology-driven design in catalysis.

Fluid transport confined at the nanoscale exhibits non-classical behaviours due to the dominance of surface forces, quantum effects, and reduced dimensionality. The high surface-to-volume ratio amplifies interfacial interactions, such as van der Waals forces, electrostatic interactions, and hydrogen bonding, leading to phenomena like enhanced viscosity, non-Newtonian flow, and altered diffusion rates.<sup>118, 119</sup> These effects are especially relevant in nanofluidic applications, where precise control over fluid transport is critical for lab-on-a-chip devices, water purification, and energy storage systems. As shown in Fig. 4c,<sup>120</sup> graphene oxide (GO) membranes, composed of stacked nanosheets, form a heterogeneous network of angstrom-scale voids that function as nanochannels for transport and separation. The hydrophilicity of GO nanosheets allows water molecules to adsorb onto the basal plane, leading to water intercalation between neighbouring nanosheets. This intercalation can expand the interlayer nanochannels, potentially compromising ion sieving efficiency. However, under pressurized water flow, the channels can be perturbed, increasing permeance while decreasing salt rejection. The tunability of GO membrane nanochannels, both in physical dimensions and chemical environments, makes them promising candidates for next-generation water-treatment membranes.

### 3.5 Mimics biological catalytic sites

As alternatives to natural enzymes, various artificial enzymes—commonly referred to as nanozymes—have been developed, including synthetic peptides, molecular catalysts, and catalytic nanomaterials. These nanozymes exhibit notable catalytic activity, robust durability, and substrate selectivity.<sup>121–123</sup> Nanoarchitectonics provides various strategies in replicating

biological catalytic sites within synthetic systems, enabling precise modulation of their properties (e.g., physical characteristics, catalytic activities, and biological effects) to meet diverse application requirements. By mimicking the structure and function of enzyme active sites, nanozymes can operate under mild conditions with high efficiency and selectivity, effectively bridging the gap between biological and synthetic catalysis.

One approach to mimicking biological catalytic sites involves replicating the catalytic microenvironment of natural enzymes by emulating the atomic and electronic structures of their active sites. Key strategies include introducing coordination sites, mimicking cofactor structures, and modifying surface functional groups to fine-tune catalytic activity. For instance, studies have demonstrated that combining coordinated metal clusters (e.g., Fe-N<sub>4</sub> and Fe-N<sub>5</sub>)<sup>124, 125</sup> as cofactors in the active site significantly enhances the catalytic performance of nanozymes. By simulating the cofactor structure of natural enzymes and incorporating atomic Fe clusters with Fe-N<sub>4</sub> as the active site (Fig. 5a), researchers have developed peroxisome-like nanozymes with high stability and biocompatibility.<sup>126</sup> These nanozymes have shown exceptional efficacy in treating conditions such as hyperuricemia and ischemic stroke.

Another strategy involves encapsulating nanozymes within membrane structures or supramolecular cages to replicate the confined environments of enzyme active sites. For example, MOFs incorporating metalloporphyrin ligands have been designed to mimic the active sites of heme-containing enzymes, such as cytochrome P450.<sup>127, 128</sup> These biomimetic MOFs exhibit high catalytic activity in oxidation reactions, closely paralleling the functionality of natural enzymes. Compared to rigid MOFs nanoarchitectures, soft polymer vesicles, characterized by their hydrophilic cavities and hydrophobic membranes, represent a versatile and robust substrate to anchor enzymes and other biomolecules. These structures offer high structural stability, adjustable permeability, and the capacity to encapsulate both hydrophilic and hydrophobic components, making them

particularly advantageous for multifunctional biomedical based-nanoreactor design. Their structural resemblance to cellular compartments renders them highly suitable for long-term operation and stimuli-responsive behaviour, enabling applications such as sustained drug delivery,<sup>129</sup> stimuli-responsive therapeutic,<sup>130</sup> multi-step cascade reactions,<sup>129, 131</sup> and the engineering of artificial organelles.<sup>132</sup>

In living organisms, the distribution of active species is often regulated through compartmentalization, where enzymes and substrates are localized within specific organelles or membrane-bound structures. Inspired by this natural strategy, soft polystyrene-encased nanoframe (PEN) reactor arrays have been developed as nanoscale "sheet-like chemosynthesis plants" for the spatially controlled synthesis of nanocrystals.<sup>133</sup> As illustrated in Fig. 5b, each individual PEN reactor has a volume in the zeptoliter range, providing a unique confined environment that enables directional inward crystallization, contrasting with conventional outward nucleation and growth observed in unconfined bulk solutions. The ~3 nm thick, soft polystyrene layer provides mechanical flexibility and selective permeability to aqueous solutes, while significantly impeding diffusion. This confinement strategy results in improved control over crystallization dynamics, particle morphology, and reaction yield. These advances underscore the versatility of nanoarchitectonics in designing biomimetic catalytic systems. By emulating the spatial, electronic, and structural complexity of enzyme active sites, synthetic nanozymes are emerging as powerful tools in biomedicine, industrial catalysis, and environmental sustainability.

### 3.6 Import external stimulation

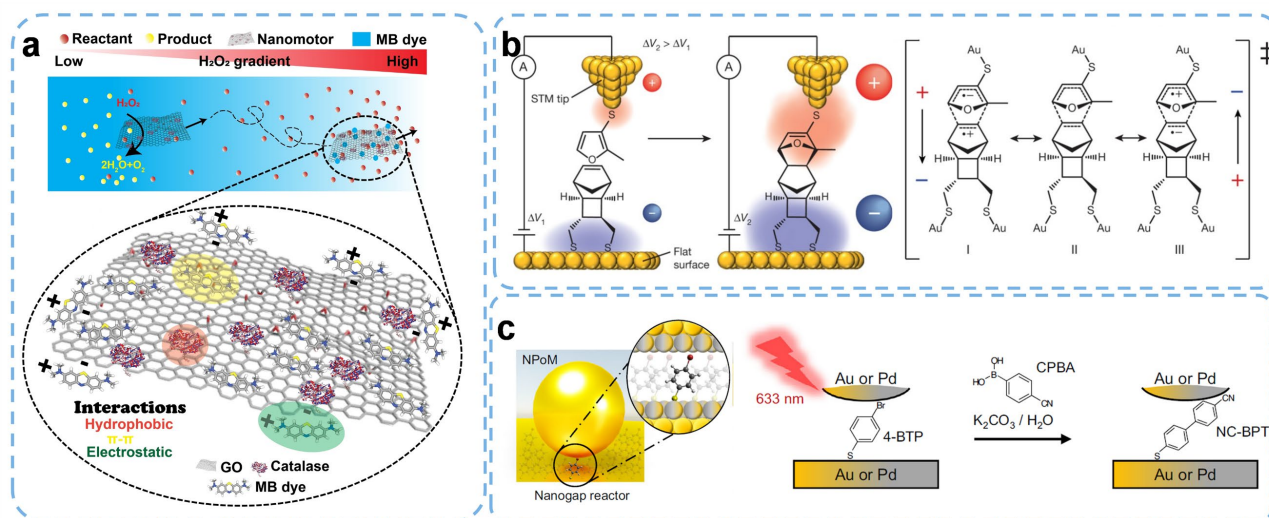
The ability to dynamically control nano-reactors through external stimuli is a key advantage of nanoarchitectonics. External stimulation, such as potential, magnetic fields, light, temperature, or chemical signals, can be used to modulate the surface properties of nano-reactors, enhance binding interactions, and modulate reaction kinetics. This approach

enables the development of adaptive nano-reactors capable of responding to changing environmental conditions, significantly outperforming conventional static catalytic systems in versatility and efficiency.

Firstly, the design of such nano-reactors relies heavily on the integration of stimuli-responsive materials, which undergo physical or chemical changes in response to external triggers. For example, photoresponsive materials like azobenzene or quantum dots exhibit conformational or electronic changes upon light irradiation, allowing optical control over reactivity. Similarly, thermoresponsive polymers such as poly(*N*-isopropylacrylamide) (PNIPAM) demonstrate phase transitions at specific temperatures.<sup>134</sup> Magnetic nanoparticles (e.g., Fe<sub>3</sub>O<sub>4</sub>) can be manipulated using magnetic fields, and pH-sensitive materials like polyelectrolytes adapt their properties based on environmental acidity or alkalinity.<sup>135, 136</sup> Incorporating such smart materials into nano-reactor architectures becomes possible to create systems that sense and respond to external stimuli with high precision and specificity.

Moreover, interfacial and structural nanoarchitectonics enables the engineering of highly responsive systems with spatial and temporal control.<sup>137</sup> Interfacial nanoarchitectonics focuses on the design and manipulation of materials at interfaces, where phenomena such as molecular orientation, self-assembly, and surface interactions can be harnessed to create adaptive systems. This includes the above-mentioned stimuli-responsive materials that be incorporated into supporting substrates to enable dynamic responses to external triggers. One compelling example involves enzyme-powered micro- and nanomotors, where supramolecular structures such as stomatocyte or tubular-shaped motors, exhibit directional motion in response to substrate gradients.<sup>138</sup> These systems harness enzymatic catalysis as a power source for autonomous propulsion. Recent innovations have demonstrated that 2D nanoarchitected enzyme systems offer exceptional reactivity and fuel efficiency. As shown in Fig. 6a,<sup>139</sup> catalase was immobilized onto GO

Fig. 6 (a) Schematic representation for the design of 2D nanobots using non-covalent hydrophobic interactions between catalase and GO. Copyright 2021, Wiley VCH. (b) The illustration of electrostatic catalysis of a Diels-Alder reaction. Copyright 2016, Nature Publishers. (c) Nanogap reactor construct for Suzuki-coupling catalytic reaction. Light-driven Suzuki-Miyaura C-C coupling reaction of 4-BTP and CPBA in the NR, resulting in C-C coupled NC-BPT as a product. Copyright 2024, Nature Publishers.



nanosheets through non-covalent interactions, resulting in 2D nanobots capable of propulsion in the presence of minimal hydrogen peroxide ( $\text{H}_2\text{O}_2$ ) as a fuel source. This bio-fuelled system highlights the potential of enzyme-driven nanoarchitectonics for creating autonomous nanoscale devices with applications in targeted drug delivery, environmental remediation, and beyond.

Beyond enzyme-powered systems, nanoarchitectonics enables the hierarchical integration of multiple functional components to construct complex and adaptable materials. One exemplary application lies in flexible and self-powered sensors for next-generation wearable electronics. Zhang and coworkers<sup>140</sup> employed a biomimetic soft–rigid hybrid strategy to fabricate a novel stretchable piezoelectric sensor, utilizing droplet-shaped hierarchical ceramics created via freeze casting on superhydrophobic surfaces. The arched ceramic microstructure effectively redistributes mechanical stress, while patterned liquid metal maintains electrical conductivity under strain. Silicone elastomers with tailored wettability and mechanical properties form a strong mechanical interlock with the ceramic framework, resulting in a robust and extensible sensor. This design breaks traditional limitations between piezoelectric efficiency and stretchability, opening new avenues for applications in soft robotics, human-machine interfaces, and biomedical monitoring.

Furthermore, a key aspect of nanoarchitecture reactor systems is their ability to control external fields within confined spaces to manipulate the kinetics and thermodynamics of non-catalyst processes. Aragonès et al.<sup>45</sup> have demonstrated that externally applied electric fields can significantly alter reaction kinetics and mechanisms. Using single-molecule scanning tunneling microscopy break junction (STM-BJ) conductance measurements shown in Fig. 6b, the authors applied localized electric fields across a Diels–Alder reaction confined within a molecular junction. Their findings revealed that both the strength and directionality of the applied field are critical in determining the reaction outcome. Specifically, an electric field strength of approximately 0.5 V/nm was sufficient to lower the activation energy by stabilizing the charge-separated transition state, leading to an enhancement in the reaction rate by nearly an order of magnitude. Furthermore, when the electric field was oriented along the dipole moment of the transition state, the reaction was effectively accelerated. In contrast, reversing the field direction suppressed the reaction, underscoring the importance of vector alignment in electrostatic catalysis. These results provide a compelling proof-of-concept for the use of electric fields to manipulate chemical reactivity at the molecular level. In addition to electric fields, trapped optical fields in plasmonic nanostructures can also influence reactants confined within molecular junctions by stabilizing charge-separated transition states and thereby modulating reaction rates and mechanisms.<sup>141</sup> In Fig. 6c, nanoparticle-on-mirror (NPoM) platforms have been developed as highly efficient nano-reactors for plasmonic catalysis. These constructs enable the observation and tracking of reaction pathways, such as the Pd-catalyzed C–C coupling reaction of molecules within nanogaps featuring different chemical surfaces. By precisely controlling

the atomic monolayer coatings of palladium on different gold crystallographic facets, the reaction kinetics and selectivity can be finely tuned for surface-bound molecules. Compared to randomly aggregated nanoparticle systems, NPoM reactors exhibit markedly enhanced catalytic performance and single-molecule resolution for tracking complex chemical transformations.

#### 4. Integrating the *in-situ* characterization and tracking techniques

Understanding the reaction mechanisms operating within confined nanoarchitectonics requires advanced *in-situ* characterization and tracking techniques that can probe dynamic processes with high spatial and temporal resolution. These methods provide critical insights into the structural, chemical, and electronic transformations occurring in real time under operational conditions. However, in practical scenarios, the choice of characterization methods depends on several factors, including the size, shape, and structure of the nano-reactors, as well as the specific reaction environment. To address the complex and dynamic nature of nanoscale systems, multi-modal characterization strategies have become indispensable. Integrating complementary methods—including optical, spectroscopic, electrochemical, and microscopic techniques—enables comprehensive monitoring of transient phenomena, intermediate states, and reaction pathways.<sup>142, 143</sup> This multi-modal approach not only enhances the accuracy of mechanistic studies but also facilitates the rational design of more efficient and tailored nano-reactors for diverse applications in catalysis, energy storage, and biomedicine.

##### 4.1 Microscopic methods

Microscopic characterization plays a foundational role in uncovering the structure-function relationships of nanoarchitecture systems. Techniques including atomic force microscopy (AFM), scanning electron microscopy (SEM), and *in-situ* transmission electron microscopy (TEM), offer powerful platforms for probing nanostructures at atomic to molecular resolution, allowing researchers to visualize the evolution of morphology, interfaces, and reaction intermediates during active processes. While these techniques have traditionally operated under high-vacuum or idealized environments, recent advances have extended their applicability to realistic operating conditions, essential for bridging the gap between laboratory studies and practical applications. For instance, surface morphology, electronic states, and oxidation/reduction behavior must be monitored in ambient or reactive environments to truly capture the complexity of working nano-reactors. Choi and colleagues<sup>144</sup> highlighted current trends in the development of surface characterization techniques and methodologies tailored to more realistic environments, as illustrated in Fig. 7. For instance, ambient pressure scanning tunneling microscopy (AP-STM) and ambient pressure X-ray photoelectron spectroscopy (AP-XPS) allow researchers to observe surface restructuring under oxidation, reduction, and catalytic conditions.<sup>145–147</sup> These techniques have revealed



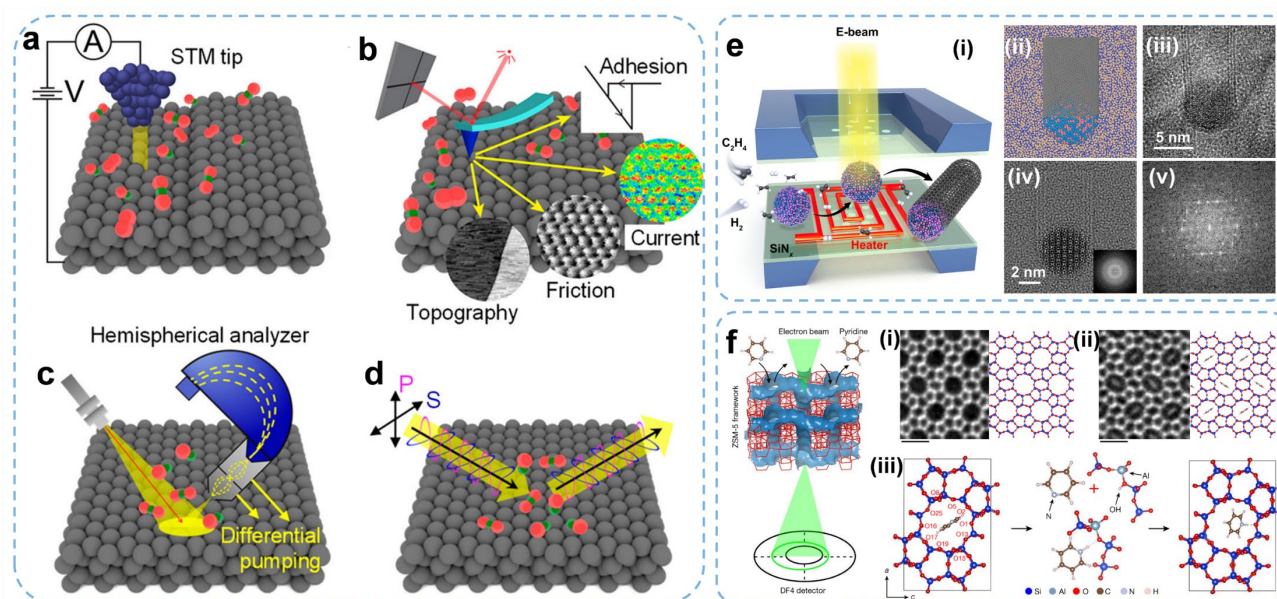


Fig. 7 Schematic illustrations of (a) AP-STM, (b) AP-AFM, (c) AP-XPS, and (d) reflection–absorption infrared spectroscopy (RAIRS). Copyright 2020, American Chemical Society. (e) Schematic and TEM image simulations of TWCNT-NP in an E-cell. (i) Schematic showing the cell structure and CNT growth process. E-beam, electron beam. (ii) Top view of the structural model of a TWCNT attached to a spherical  $\text{Co}_3\text{W}_3\text{C}$  NP with a diameter of 5 nm situated on a 30-nm-thick  $\text{SiN}_x$  membrane. (iii) Simulations of the HRTEM image and corresponding diffractogram of the TWCNT– $\text{Co}_3\text{W}_3\text{C}$  NP in (ii). (iv and v) Experimental HRTEM image and corresponding diffractogram of a TWCNT growing from a cubic Co–W–C NP in the E-cell. Copyright 2022, AAAS. (f) Schematics of *in-situ* iDPC-STEM imaging of the pyridines adsorbed in ZSM-5 channels. iDPC-STEM images of empty ZSM-5 straight channels (i) and the channels after the saturated pyridine adsorption (ii), compared with the structural models in the [010] projection. Scale bars, 1 nm. iii, Calculated pyridine configurations in the channels with and without acid sites, respectively. After the acid site is set at O1 (as numbered), a protonated pyridine will bond with the acid site by electrostatic interaction. Copyright 2022, Nature Publishers.

critical insights into the formation of reactive interfaces between metal skins and oxide clusters, a process observed on both single-crystal surfaces and bimetallic nanoparticles. Such interfaces have been identified as key elements in enhancing catalytic activity, underscoring their importance in designing efficient nano-reactors. Additionally, ambient pressure atomic force microscopy (AP-AFM) has emerged as a powerful tool for studying morphological, mechanical, and charge transport properties during catalytic and energy conversion processes.<sup>148</sup> For example, AP-AFM studies of single-crystal perovskite surfaces have provided atomic-scale insights into degradation processes, which are critical for improving the durability of materials used in energy applications.<sup>149</sup> Furthermore, the integration of hot electron detection techniques has enabled real-time tracking of chemical reactions across metal-oxide interfaces, providing valuable information on charge transfer processes that govern reaction kinetics.

TEM is a powerful technique capable of characterizing microstructures and compositions of nanomaterials at the atomic level. By enabling the visualization of both atomic structures and their dynamical evolution under gas environments and high temperatures, *in-situ* TEM has become an indispensable tool for elucidating the growth mechanisms of carbon nanotubes (CNTs).<sup>150, 151</sup> With the ability to supply a controlled gaseous environment and precise temperature regulation, *in-situ* TEM can effectively mimic the chemical vapor deposition (CVD) growth of CNTs from catalytic precursors and record the multi-phase reactions in real time. The catalytic growth mechanisms of CNTs, as revealed by *in-situ* TEM under

realistic conditions, are discussed across multiple scales—from fundamental thermodynamics and kinetics to detailed nucleation, growth, and termination processes. This includes insights into the state and phase of active catalysts, the interfacial connections between the catalyst and the growing CNTs, and the catalyst-related growth kinetics of CNTs. For instance, as illustrated in Fig. 7e,<sup>152</sup> the growth process of CNTs from a Co–W–C solid alloy catalyst at atmospheric pressure was investigated using a windowed gas cell within a Cs-corrected TEM. The active phase of the Co–W–C catalyst was identified as a single-phase cubic  $\eta$ -carbide phase, which remained stable and unchanged throughout the CNT growth process. Interestingly, the observed rotation of catalyst nanoparticles suggested weak interfacial interactions with the growing CNTs, offering insights into mobility and morphological stability of the catalyst during growth. These observations highlight the power of *in-situ* TEM in capturing intricate real-time transformations at the nanoscale, enabling better control over catalyst design and synthesis strategies.

Electron microscopy is poised to achieve real-space characterizations of lattice structures with atomic resolution, a capability that extends to imaging small molecules. Shen et al. demonstrated this breakthrough by reporting the atomic imaging of single pyridine and thiophene molecules confined within the channels of zeolite ZSM-5 using integrated differential phase contrast scanning transmission electron microscopy (iDPC-STEM), as illustrated in Fig. 7f.<sup>77</sup> Pyridine and thiophene are two typical probe molecules known to interact strongly with the Brønsted acid sites in zeolites. At these acid



sites, the atomic rings of these molecules are statically oriented in a manner suitable for imaging, enabling the visualization of molecular behaviours and interactions directly from static images and even during *in-situ* experiments. In this study, pyridine and thiophene confined within zeolite ZSM-5 serve as model molecules to explore the application of advanced imaging techniques in molecular physics and chemistry. Based on static iDPC-STEM images, the six-membered ring of a single pyridine molecule and the sulfur atom in a single thiophene molecule were precisely located, revealing host–guest interactions at the acid sites within the ZSM-5 channels. This study exemplifies how advanced electron microscopy techniques can extend beyond imaging static structures to directly visualizing host–guest interactions at the atomic level—even under *in-situ* conditions. These capabilities are transformative for exploring molecular behaviours in confined nanoenvironments, opening avenues for real-time mechanistic studies in molecular catalysis, adsorption, and separation.

#### 4.2 Optical and spectroscopic methods

Optical and spectroscopic methods are indispensable tools for *in-situ* characterization, offering non-invasive, high-resolution analysis of chemical bonding, phase transitions, and reaction dynamics.<sup>153</sup> In this section, we highlight several key techniques, including Raman spectroscopy, infrared (IR) spectroscopy, and single-molecule fluorescence spectroscopy which have proven invaluable for probing molecular and structural transformations in real time within confined nanoarchitectures.

Spectroscopic techniques, such as infrared (IR) spectroscopy and Raman spectroscopy, are particularly effective for structural characterization of molecular anchored in nanostructures under ambient conditions. In Raman spectroscopy, the interaction of light with molecular vibrations produces distinctive spectral fingerprints, which are greatly amplified in the presence of nanostructures via surface-enhanced Raman scattering (SERS). This enhancement enables single-molecule sensitivity, making Raman spectroscopy highly effective for identifying chemical bonds and monitoring reaction intermediates.<sup>141</sup> As a model of NP-on-mirror (NPoM) geometry shown in Fig. 8a, a self-assembled monolayer (SAM) is confined between a gold nanoparticle and a metallic mirror, forming a nanogap that supports localized surface plasmon resonances. These plasmons generate hot carriers that trigger redox reactions in adjacent molecules.<sup>154</sup> This model has been employed to study the catalytic oxidation of CO on gold nanoparticles confined within mesoporous silica, revealing the formation of intermediate species and their role in the reaction mechanism.<sup>155</sup> To overcome the material and surface limitations inherent in conventional SERS, shell-isolated nanoparticle-enhanced Raman spectroscopy (SHINERS) has emerged (Fig. 8b). In SHINERS, plasmonic gold nanoparticles are coated with ultrathin, pinhole-free silica shells, which preserve the enhanced electromagnetic field while preventing direct chemical interaction with the analyte. This strategy enables Raman signal amplification on virtually any substrate and morphology, extending the applicability of SERS across diverse catalytic platforms. Similarly, Raman spectroscopy has been used to monitor the reduction of nitroaromatics in MOF-based

nano-reactors, elucidating the contributions of metal nodes and organic linkers to the catalytic process.<sup>156, 157</sup> This work underscores the importance of confined environments in enhancing catalytic activity. At the macroscopic level, combined *in-situ* Raman and <sup>1</sup>H NMR spectroscopy has been used to investigate solvent exchange dynamics, providing a comprehensive understanding of reaction environments.<sup>158</sup>

Molecular junctions, fabricated by creating nanoscale gaps between metal nanoelectrodes, can effectively exhibit properties akin to face-to-face coupled antennas. This configuration enables surface-enhanced Raman scattering (SERS) characterization of bridging molecules within the nanogap, where the molecules act as "hotspots" for enhanced Raman signals.<sup>159, 160</sup> Since Tian et al. first reported the SERS study of molecular junctions by combining SERS with mechanically controllable break junction (MCBJ) techniques (Fig. 8c),<sup>161</sup> the integration of electrical and enhanced Raman spectroscopic methods for characterizing single-molecule junctions has gained significant traction. This approach allows researchers to simultaneously probe electronic and vibrational properties, providing a comprehensive understanding of molecular behaviour at the nanoscale. Building on this foundation, Bi et al.<sup>162</sup> advanced the field by modifying the STM tip with a gold-covered tetrahedral glass (t-tip). This innovative design allows a laser to be introduced into the molecular junction through the tetrahedral glass (Fig. 8d). Using this setup, they demonstrated voltage-controlled conformational switching in molecular junctions, showcasing the dynamic interplay between electrical stimuli and molecular structure. This nanostructure-based molecular junction, combined with real-time Raman monitoring, enables the simultaneous measurement of electronic and vibrational properties. Such dual-characterization capabilities offer unprecedented insights into molecular behaviour, including conformational changes, charge transfer processes, and chemical interactions at the single-molecule level.

Other spectroscopic techniques, such as *in-situ* diffuse reflectance Fourier transform infrared spectroscopy (DRIFT), have been employed to unveil electron transfer processes during catalytic reactions, providing critical insights into reaction mechanisms. For instance, Parambil and coworkers<sup>163</sup> developed an integrated system by grafting a molecular photosensitizer and a catalyst within the porous structure of a zirconium-based MOF (Zr-MOF) for CO<sub>2</sub> reduction. The confined space of the Zr-MOF nanopores provided a rigid platform that facilitated the proximal alignment of the photosensitizer and the molecular catalyst. This spatial arrangement enabled rapid electron transport from the photosensitizer to the catalyst, significantly enhancing the reaction kinetics. By tracking carbonyl IR stretching frequencies, the researchers confirmed efficient real-time electron transfer, emphasizing the strength of DRIFT for probing reaction intermediates and pathways. The DRIFT technique is also reported to observe the hyponitrite radical intermediates during NO disproportionation at MOF-supported mononuclear copper sites.<sup>164</sup> These findings highlight the critical role of spectroscopic techniques in

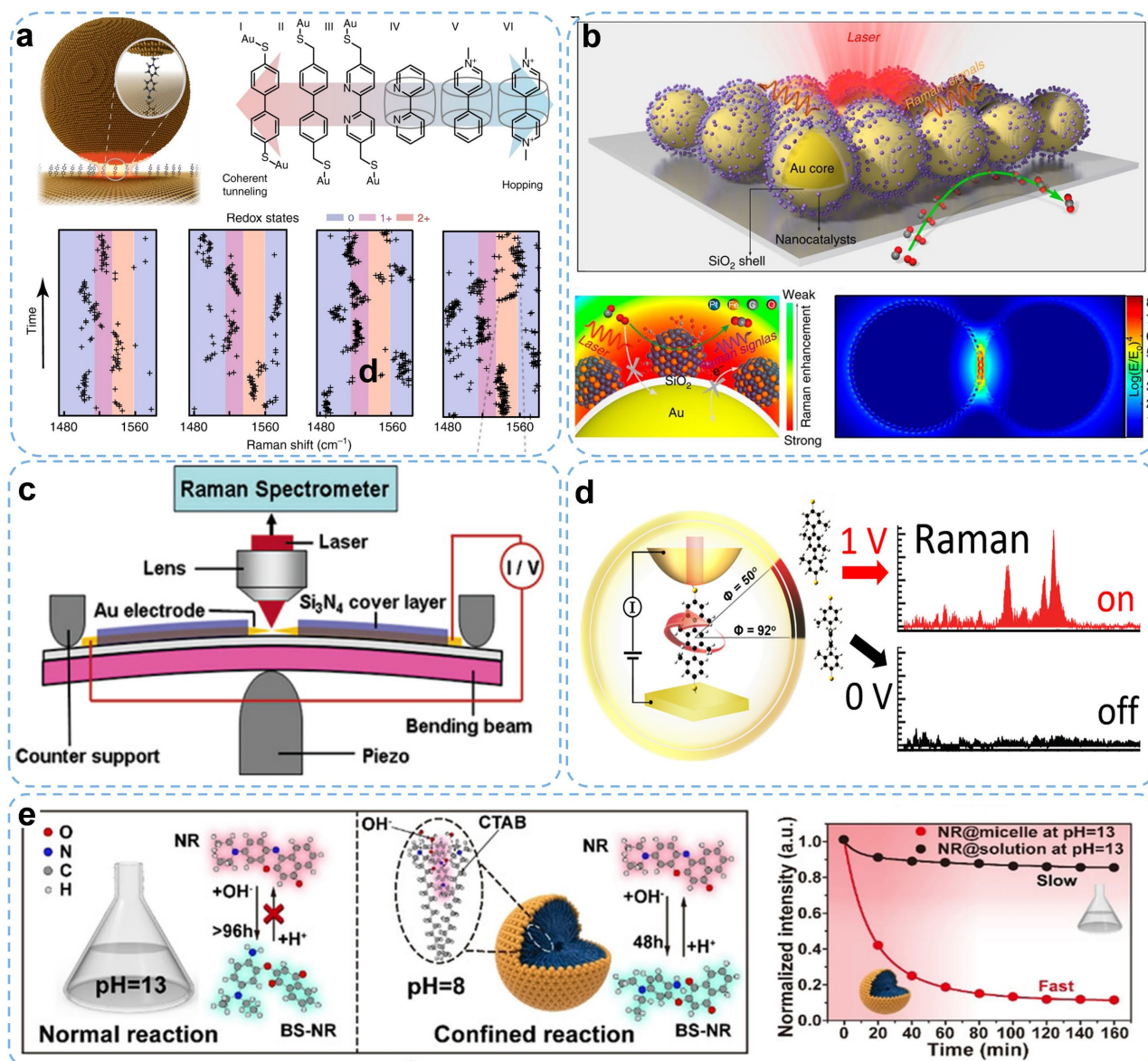


Fig.8 (a) Plasmon generated hot charge carrier transport in a nanoparticle-on-mirror geometry and evolving vibrational peak positions from several NPoM constructs compared to redox states of six different molecular junctions. Copyright 2017, Nature Publishers. (b) The Au-core silica-shell nanocatalyst-satellite architecture of SHIN-enhanced Raman spectroscopy (SHINERS)-satellite structures, and the mechanism for CO oxidation over PtFe bimetallic nanocatalysts revealed by our SHINERS-satellite method. Copyright 2017, Nature Publishers. (c) Schematic drawing of the experimental setup of combined Raman and MCBJ. Copyright 2006, American Chemical Society. (d) Voltage-driven Raman switching in a molecular junction spectroscopy setup. Copyright 2018, American Chemical Society. (e) Chemical reactions in free space (solution) are contrasted with those in a confined space (CTAB micelle) and the normalized fluorescence intensity of NR (647 nm) changes as a function of time in both solution and micelles (pH 13). Copyright 2021, Wiley VCH.

identifying transient intermediates and elucidating intricate reaction mechanisms.

Fluorescence spectroscopy is another versatile tool for dynamically monitoring reactions, particularly in systems involving fluorescent probes or catalysts.<sup>165</sup> In TiO<sub>2</sub>-based nano-reactors, fluorescence spectroscopy has enabled real-time monitoring of photocatalytic degradation of organic pollutants by tracking the formation and consumption of reactive oxygen species (ROS).<sup>166, 167</sup> This technique also provides valuable information about bond cleavage and reformation events, particularly within confined nanospaces.<sup>168</sup> As illustrated in Fig. 8e, individual fluorescent molecules were confined within cetyltrimethylammonium bromide (CTAB) micelles. Spatial

confinement within the micelles suppresses molecular motion, reducing energy dissipation and minimizing unproductive energy consumption during reactions. For instance, breaking the C=N bond of Nile Blue is challenging in bulk solution and typically requires harsh conditions. However, when the same reaction was conducted within the confined nanospace of a micelle, a significant colour change was observed at a mild pH of 8, accompanied by a blue shift in the absorption and emission spectra of the molecule. This spectral shift indicates the cleavage of the C=N bond, leading to the disruption of the molecular conjugate system. Moreover, as discussed in Section 3.5, the compartmentalization of reactions within cells is essential for life. Single-molecule fluorescence spectroscopy

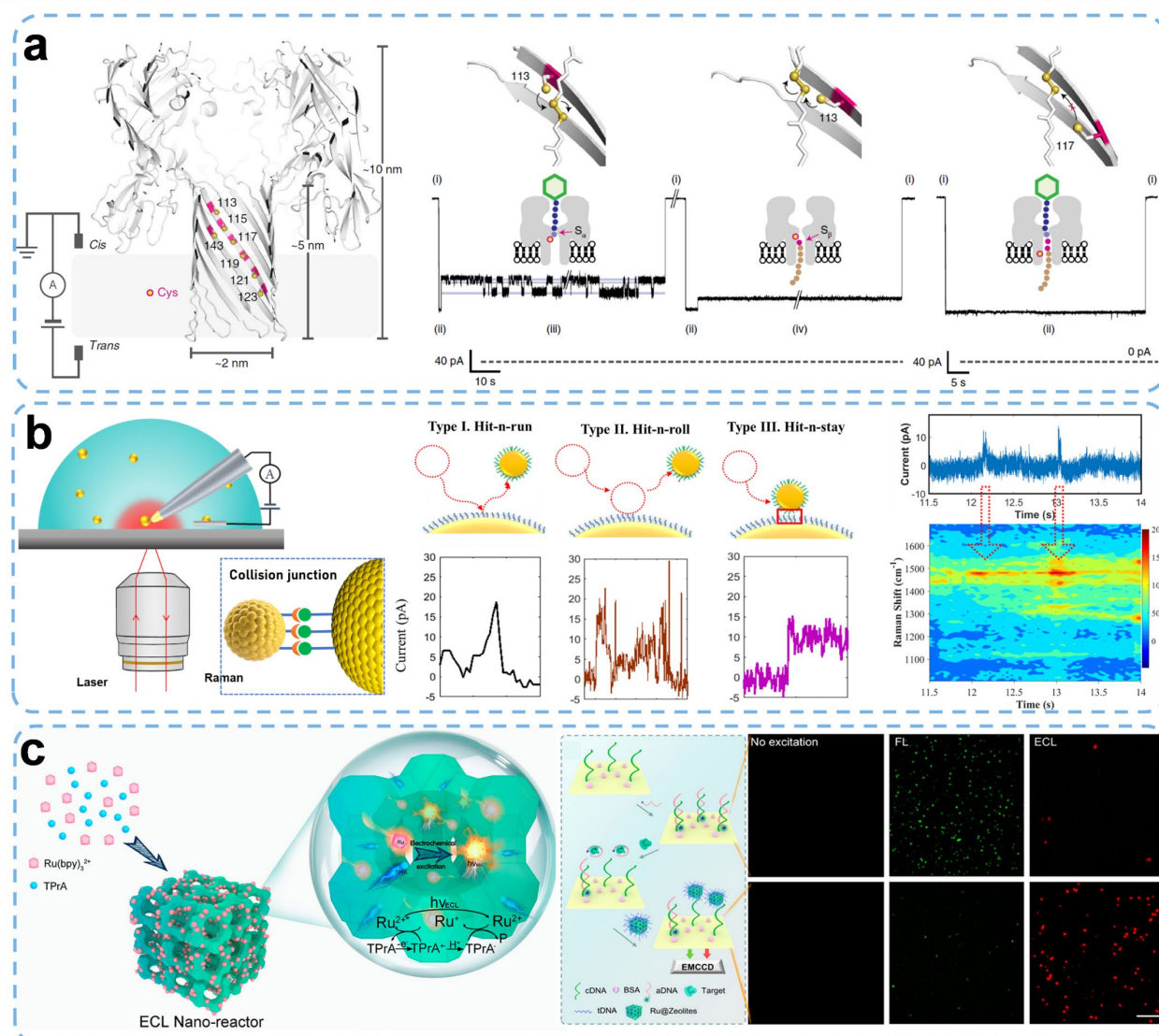


Fig. 9 (a) Schematic illustration of a catalytic site-selective substrate processing in a nanopore confined space. Cysteines (Cys, pink) located on one of the seven  $\alpha$ HL subunits in the  $\alpha$ -HL nano-reactor provides nucleophilic thiolates. Copyright 2019, Nature Publishers. (b) Schematic illustration of NP collision events and the corresponding current responses: (I) hit-n-run, (II) hit-n-roll, (III) hit-n-stay. (Right) The simultaneously recorded time resolved SERS trajectory and I-t trace. Copyright 2021, American Chemical Society. (c) The schematic mechanism for the nanoconfinement-enhanced ECL reaction at single nano-reactors and dual-signal imaging platform (FL and ECL) to image the target molecules. Copyright 2023, American Chemical Society.

plays a critical role in studying compartmentalized chemical reactions *in vitro*.<sup>169</sup> By labeling engineered encapsulins with fluorescent tags, researchers can monitor catalytic processes in real time within confined cellular environments. This approach demonstrates that engineered encapsulins can serve as hosts for transition metal catalysis within living cells and opens new avenues for developing synthetic systems that mimic the efficiency and selectivity of natural enzymatic reactions.

#### 4.3 Electrochemical tracking platforms

Electrochemical techniques are highly advantageous for tracking chemical reactions in real time due to their ability to provide easy-to-process sensor readouts (e.g., current or potential) and tunable experimental parameters.<sup>170</sup> In this section, we discuss several electrochemical-based tracking techniques for studying charge transfer, reaction dynamics, and local electrochemical processes within confined nano-reactors.

From both experimental and theoretical perspectives, electroanalytical behaviours in confined spaces is primarily governed by the properties of the electrode interface, including its electrical, compositional, and structural characteristics. Key electrochemical parameters, such as mass transport, reactant distribution near the electrode, and interface dynamics, are profoundly affected by the surface confinement.<sup>170</sup> Given that all electrochemical reactions occur at the interface between ionic and electronic conductors, interfacial phenomena are central to defining system behaviour. Conventional electrochemical techniques, which record electrical signals (current and potential) with high sensitivity, provide detailed interfacial migration of active species at sub monolayer levels.<sup>171</sup> These methods reveal electrochemical kinetics, changes in analyte concentration, and the catalytic capabilities of electrodes.

Recent advancements in stochastic single-entity electrochemistry (SEE) have made it possible to monitor individual entities, such as single cells, single particles, and even single molecules, at the nanoscale precision.<sup>172-174</sup> This is achieved through well-defined interfaces, including micro-/nanoelectrodes,<sup>175, 176</sup> nanopipettes,<sup>177</sup> nanopores/nanochannels,<sup>178, 179</sup> and nanogaps,<sup>180</sup> which effectively isolate and interact with individual moving entities. For example, Bayley's group<sup>181</sup> demonstrated site-selective and regioselective reactions by confining macromolecular disulfide substrates within cysteine mutants of  $\alpha$ -hemolysin ( $\alpha$ -HL) nanopores (Fig. 9a). Under an applied electric field, the substrates elongated within the tubular protein nanopore, allowing precise thiol–disulfide interchange reactions at specific locations along the nanopore. This confinement enabled atomic-level precision in reaction control, which is unachievable in bulk solutions.

In another typical SEE, collision electrochemistry<sup>182</sup> investigates the dynamic interaction of nanoparticles (NPs) with electrode surfaces. Each collision event creates single- or few-molecule junctions, forming NP-molecule-substrate architectures. These architectures, termed "colliding molecular junctions", provide insights into molecular dynamics at the nanoscale (Fig. 9b).<sup>183</sup> Real-time monitoring of current, charge, or related quantities associated with blockade, oxidation/reduction, and electrocatalysis offers a direct strategy to track collision activity.<sup>184</sup> Stochastic collision models, such as "hit-and-run," "hit-and-roll," and "hit-and-stay," produce distinguishable current changes, including single spikes, cluster spikes, and staircase signals (Fig. 9b). Statistical analysis of current amplitude, duration, and integrated charge from current-time (i-t) profiles yields quantitative insights into reaction kinetics, charge transfer, and single-molecule events. For instance, Compton and coworkers<sup>185</sup> investigated the dopamine oxidation on graphene nanoplatelets and found enhanced collision currents attributed to catalytic oxidation of adsorbed dopamine. However, the accumulation of oxidative products on the nanoplatelets eventually blocked electron transfer, leading to partial oxidation. This study provided evidence that electron transfer occurs on the surface of graphene nanoplatelets rather than through them, advancing the understanding of dopamine oxidation mechanisms. In another example, Wang et al.<sup>186</sup> demonstrated direct ion migration behaviour of single charged nanoparticles using a plasmonic-based transient microscopic method. They studied deviations in electric double-layer dynamics from classical resistance–capacitance models and proposed a transient theory to explain these phenomena.

Despite the insights provided by SEE, its limited spatial resolution poses challenges in resolving structural features of molecular junctions. To overcome this, hybrid approaches integrating electrochemistry with spectroscopic techniques (e.g., electrochemical surface-enhanced Raman spectroscopy, EC-SERS) and molecular dynamics (MD) simulations have been developed. In our previous work,<sup>187</sup> we combined EC-SERS with nanoparticle collision studies to monitor the dynamic evolution of amide bond formation during single-gold nanoparticle (GNP) collision events with millisecond time resolution. The transient

Raman peaks identified key intermediates, providing mechanistic insights into amide bond formation. This approach enables real-time monitoring of covalent bond transformations and opens new avenues for studying chemical reactions at the single-molecule level.

Another important electrochemical method is electrochemiluminescence (ECL), which provides highly sensitive and selective visualization of reaction intermediates through light emission generated during redox processes.<sup>188</sup> For example, Lu et al. developed  $\text{Ru}(\text{bpy})_3^{2+}$ -doped nanoporous zeolite nanoparticles ( $\text{Ru@zeolite}$ ) as nano-reactors to capture single photons emitted from single-molecule ECL reactions.<sup>189</sup> As shown in Fig. 9c, confinement within nanopores increased the interaction and collision probabilities between radicals (generated by co-reactant tripropylamine, TPrA), enhancing photon generation and ECL emission. This  $\text{Ru@zeolite}$  nano-reactor was further used to construct a single-protein imaging platform combining fluorescence (FL) and ECL. In the absence of target proteins, no bright spots were observed in FL or ECL images. However, upon target protein binding, ECL counts increased dramatically, while FL spots decreased, demonstrating the platform's specificity and sensitivity. Other electrochemical imaging techniques, such as scanning electrochemical microscopy (SECM),<sup>190</sup> scanning electrochemical cell microscopy (SECCM),<sup>191</sup> and scanning ion conductance microscopy (SICM),<sup>192</sup> have enabled the visualization and sensing of single-entity activities by recording spatially dependent fluxes of reactants, products, or intermediates. These techniques provide high-resolution spatial and temporal information, essential for understanding localized reactivity and interfacial dynamics.

Electrochemical tracking techniques, including SEE, ECL, and electrochemical imaging, serve as powerful tools for studying charge transfer, reaction dynamics, and interfacial processes at the nanoscale. These techniques are indispensable for optimizing the design and performance of nano-reactors in sensing, energy storage, and catalytic applications, such as fuel cells and batteries. Furthermore, the integration of electrochemical methods with structural and spectroscopic characterization (Raman,<sup>187</sup> AFM,<sup>193</sup> mass spectrometry,<sup>194</sup> NMR spectroscopy,<sup>195, 196</sup> et al.), researchers can achieve a deeper understanding of single-entity behaviour and reaction mechanisms, paving the way for innovative applications in confined nanoarchitectonics and the broad materials science.<sup>197</sup>

#### 4.4 Other techniques

Scattering-based techniques, including X-ray diffraction (XRD), dynamic/static light scattering (DLS/SLS), and small/wide-angle X-ray scattering (SAXS/WAXS), are widely used spatially averaged methods that provide quantitative insights into crystallization kinetics and bulk structural properties.<sup>198</sup> These methods are particularly valuable for determining reaction rate constants, activation energies, and structural parameters, such as crystal size, lattice spacing, and morphology. For example, *in-situ* XRD has been instrumental in studying the crystallization of zeolites and MOFs, revealing the formation of intermediate phases and their transformation into the final product.<sup>199, 200</sup> In



the case of ZSM-5 zeolite synthesis, *in-situ* XRD studies under varying conditions—such as SiO<sub>2</sub> to Al<sub>2</sub>O<sub>3</sub> ratio, pH, crystallization time, and temperature—have provided detailed insights into nucleation and growth mechanisms. These insights have facilitated the rational optimization of synthesis protocols to enhance material properties, particularly for catalytic applications.

The global proliferation of synchrotron radiation (SR) facilities has significantly advanced the development of high-brilliance, SR-based spectroscopic tools, particularly for probing interfacial and surface phenomena in aqueous and electrochemical environments.<sup>201, 202</sup> Among these, X-ray absorption fine structure spectroscopy (SR-XAFS) and Fourier transform infrared spectroscopy (SR-FTIR) have emerged as powerful non-invasive techniques for studying electrocatalytic systems under realistic operating conditions. Chen and colleagues<sup>203</sup> have highlighted the utility of these methods in monitoring the atomic-level evolution of single-atom nickel (Ni) catalysts at solid–liquid electrochemical interfaces (SLEIs) during the oxygen reduction reaction (ORR). These *in situ* analyses revealed the transformation of Ni into a near-free-atom state, thereby offering mechanistic insights into the structure–activity relationship of single-atom catalysts during electrocatalysis.<sup>204</sup> Another technique with emerging relevance to confined systems is the crossed molecular beam (CMB) method,<sup>205, 206</sup> traditionally used to study gas-phase molecular collisions. When adapted to simulate nano-reactor environments, the CMB approach enables two molecular beams to intersect within a confined spatial domain, replicating the limited reaction volumes found in nanoscale systems. By analyzing the trajectories and scattering patterns of reaction products—typically detected using time-of-flight mass spectrometry or velocity map imaging—researchers can obtain detailed information on reaction dynamics, product distributions, and energy transfer processes under confinement. This methodology is especially useful for understanding how spatial restriction alters chemical reactivity, including shifts in activation barriers, stabilization of reactive intermediates, and changes in product selectivity.<sup>43</sup> For example, using CMB experiments, one can investigate how molecular confinement modulates reaction pathways that would otherwise proceed differently in bulk-phase or gas-phase conditions. When coupled with complementary techniques such as high-resolution spectroscopy or advanced microscopy, the CMB approach offers a comprehensive view of reaction mechanisms in confined nanoscale environments.

## 5. Summary and perspectives

This review article introduced various confined nanostructures with functional properties used as nano-reactors, highlighting their unique capabilities in controlling chemical reactions, material synthesis, and energy conversion at the nanoscale. Confined nanoarchitectonics, which involves the precise design and manipulation of nanoscale environments, has emerged as a powerful strategy for creating highly efficient and selective nano-reactors. These systems leverage the principles of spatial

confinement, interfacial effects, and nanoscale phenomena to achieve unprecedented control over reaction kinetics, selectivity, and product distribution. A wide range of confined architectures from molecule cages, supramolecular assemblies, natural/artificial nanocavities, to porous materials and hollow nanostructures enabled significant progress in catalysis, energy storage, drug delivery, and environmental remediation. Researchers are increasingly focused on tailoring the local environments at the nanoscale to enable the fine-tuning of reaction pathways, facilitates the formation of otherwise unstable species, and opens new avenues for designing highly efficient and selective catalytic systems.

The integration of *in-situ* characterization and tracking systems has been instrumental in advancing our understanding of nanoscale processes within these confined environments. Techniques such as *in-situ* microscopic, optical, spectroscopic, electrochemical and scattering-based techniques have provided real-time, high-resolution insights into the dynamic behaviour of reactants, intermediates, and products within nano-reactors. These tools have not only elucidated fundamental mechanisms but also guided the rational design of more efficient and functional nano-reactor systems. Furthermore, the development of multimodal characterization approaches, combining multiple analytical techniques, has expanded the analytical capabilities needed to investigate complex nanoscale phenomena under operationally relevant conditions.

Despite these advancements, the field of confined nanoarchitectonics for nano-reactors is still in its early stages, and several challenges must be addressed to fully realize its potential. First, capturing the dynamic processes occurring within nano-reactors at the atomic and molecular level is inherently difficult due to limitations in spatial and temporal resolution. Many reactions within confined nanoenvironments involve ultrafast events (femtosecond to nanosecond timescales) and nanoscale structural rearrangements, which require real-time, high-resolution monitoring tools capable of operating under operando conditions. However, existing *in-situ* techniques—such as TEM, AFM, and X-ray spectroscopy—often face trade-offs between spatial resolution, temporal resolution, and environmental compatibility. For instance, high-resolution imaging may require vacuum environments that do not reflect realistic operating conditions of liquid-phase or gas-solid reactions. Furthermore, continuous long-term monitoring is hindered by instrumental drift, radiation damage, and signal-to-noise limitations, especially when targeting sub-nanometer resolution in highly dynamic systems. These constraints limit our ability to fully understand reaction pathways, transient intermediates, and feedback mechanisms within confined architectures.

Second, the scaling-up of nano-reactors from laboratory prototypes to practical, real-world applications presents formidable technical and economic hurdles. Nano-reactors often rely on precision-engineered structures—such as hollow nanotubes, porous frameworks, or hybrid interfaces—that are challenging to reproduce at industrial scale with consistent quality, yield, and reproducibility. Moreover, ensuring structural stability and uniform performance across large

batches or integrated systems remains a significant obstacle. As nano-reactors are scaled up, maintaining the delicate balance of confinement effects, reactant diffusion, and catalyst accessibility becomes increasingly complex. There are also challenges related to integration with existing process technologies, cost-effectiveness of fabrication, and regulatory and environmental considerations—particularly when dealing with potentially toxic or non-degradable nanomaterials.

Looking ahead, addressing these challenges aligns with the core philosophy of nanoarchitectonics, which emphasizes the rational design and assembly of functional systems through the integration of nanoscale processes, bridging disciplines to create transformative materials and devices. One promising direction is the development of advanced fabrication techniques that offer greater precision, scalability, and cost-effectiveness. Methods such as 3D nanoscale printing, self-assembly, and bio-inspired fabrication could enable the creation of more complex and functional nano-reactor architectures. Moreover, the integration of machine learning and artificial intelligence into the design and optimization process could revolutionize the discovery and tuning of nano-reactor systems, accelerating development cycles and revealing novel structure-function relationships. These data-driven tools can efficiently process vast datasets to identify non-obvious structure-function relationships, predict optimal design parameters, and accelerate materials discovery. For instance, machine learning models trained on experimental and simulated data can assist in screening millions of candidate nanostructures for desired catalytic performance, stability, or transport characteristics.

In parallel, advances in correlative and multimodal characterization platforms are expected to enhance the spatial and temporal resolution of *in-situ* techniques. The development of operando-compatible instruments, such as environmental TEM, liquid-phase AFM, and synchrotron-based X-ray spectroscopy, is expanding our capacity to visualize and quantify confined reactions under realistic conditions. Ultrafast spectroscopy, liquid-phase electron microscopy, and electrochemical based-imaging can further enable the capture of fleeting intermediates and dynamic transformations at the nanoscale. Integration of these techniques with machine learning and artificial intelligence-guided data processing will facilitate more comprehensive and interpretable analysis, overcoming traditional limitations imposed by data complexity or acquisition constraints.

Another key perspective is the emergence of smart and adaptive nano-reactors that can dynamically respond to changing reaction conditions. By incorporating stimuli-responsive materials and feedback mechanisms, these systems could achieve real-time adjustment of reaction parameters, enhancing their efficiency and selectivity. Such advancements would be particularly valuable in applications such as catalysis, where reaction conditions can vary significantly. Sustainability will also play a central role in shaping the future of nano-reactor technology. The development of green synthesis methods, the use of renewable materials, and the design of energy-efficient nano-reactors will be essential for minimizing the

environmental impact of these systems. Additionally, research into the recycling and reuse of nano-reactors will be critical for ensuring their long-term viability and reducing waste.

In conclusion, confined nanoarchitectonics for nano-reactors represents a rapidly evolving field with immense potential to transform a wide range of industries. By leveraging the unique properties of nanoscale confinement and advancing *in-situ* characterization techniques, researchers can unlock new opportunities for precision engineering and innovation. While challenges remain, the continued pursuit of advanced fabrication methods, smart and adaptive systems, sustainable practices, and interdisciplinary collaboration will pave the way for a new era of nanoscale science and technology. As the field progresses, it holds the promise of addressing some of the most pressing global challenges, from energy sustainability to healthcare and environmental protection, making it a cornerstone of future technological advancements.

## Author contributions

N.K.: conceptualization, writing, review & editing. K.A.: conceptualization, writing, review & editing, funding acquisition.

## Conflicts of interest

There are no conflicts to declare.

## Acknowledgements

This study was partially supported by the Japan Society for the Promotion of Science KAKENHI (Grant Numbers JP20H00392, JP23H05459 and JP24KF0272).

## References

1. B. M. Weckhuysen, S. Kitagawa and M. Tsapatsis, *ChemPhysChem*, 2018, **19**, 339-340.
2. B. Zhou, Y.-Q. Wang, C. Cao, D.-W. Li and Y.-T. Long, *Sci. China Chem.*, 2018, **61**, 1385-1388.
3. A. Küchler, M. Yoshimoto, S. Luginbühl, F. Mavelli and P. Walde, *Nat. Nanotechnol.*, 2016, **11**, 409-420.
4. S. H. Petrosko, R. Johnson, H. White and C. A. Mirkin, *J. Am. Chem. Soc.*, 2016, **138**, 7443-7445.
5. M. Viciano-Chumillas, M. Mon, J. Ferrando-Soria, A. Corma, A. Leyva-Pérez, D. Armentano and E. Pardo, *Acc. Chem. Res.*, 2020, **53**, 520-531.
6. L.-M. Cao, J. Zhang, X.-F. Zhang and C.-T. He, *Chem. Sci.*, 2022, **13**, 1569-1593.
7. X. Han, Q. Gao, Z. Yan, M. Ji, C. Long and H. Zhu, *Nanoscale*, 2021, **13**, 1515-1528.
8. K. Ariga, X. Jia, J. Song, J. P. Hill, D. T. Leong, Y. Jia and J. Li, *Angew. Chem., Int. Ed.*, 2020, **59**, 15424-15446.
9. K. Ariga, *Bull. Chem. Soc. Jpn.*, 2024, **97**, uoad001.
10. Y. Sugimoto, P. Pou, M. Abe, P. Jelinek, R. Pérez, S. Morita and O. Custance, *Nature*, 2007, **446**, 64-67.
11. S. Kawai, O. J. Silveira, L. Kurki, Z. Yuan, T. Nishiuchi, T. Kodama, K. Sun, O. Custance, J. L. Lado and T. Kubo, *Nat. Commun.*, 2023, **14**, 7741.

12. M. Aono and K. Ariga, *Adv. Mater.*, 2016, **28**, 989-992.
13. Y. Hashikawa and Y. Murata, *Bull. Chem. Soc. Jpn.*, 2023, **96**, 943-967.
14. K. Sun, N. Cao, O. J. Silveira, A. O. Fumega, F. Hanindita, S. Ito, J. L. Lado, P. Liljeroth, A. S. Foster and S. Kawai, *Sci. Adv.*, 2025, **11**, eads1641.
15. K. Ariga, M. Nishikawa, T. Mori, J. Takeya, L. K. Shrestha and J. P. Hill, *Sci. Technol. Adv. Mater.*, 2019, **20**, 51-95.
16. Y. Yamamoto, S. Kushida, D. Okada, O. Oki and H. Yamagishi, *Bull. Chem. Soc. Jpn.*, 2023, **96**, 702-710.
17. H. Wang, Z. Feng and B. Xu, *Angew. Chem.*, 2019, **131**, 10532-10541.
18. J. Song, K. Kawakami and K. Ariga, *Adv. Colloid Interface Sci.*, 2025, 103420.
19. C. L. Gnawali, S. Manandhar, S. Shahi, R. G. Shrestha, M. P. Adhikari, R. Rajbhandari, B. P. Pokharel, R. Ma, K. Ariga and L. K. Shrestha, *Bull. Chem. Soc. Jpn.*, 2023, **96**, 572-581.
20. G. Chen, M. Isegawa, T. Koide, Y. Yoshida, K. Harano, K. Hayashida, S. Fujita, K. Takeyasu, K. Ariga and J. Nakamura, *Angew. Chem., Int. Ed.*, 2024, **63**, e202410747.
21. O. N. Oliveira Jr, L. Caseli and K. Ariga, *Chem. Rev.*, 2022, **122**, 6459-6513.
22. J. Song, A. Jancik-Prochazkova, K. Kawakami and K. Ariga, *Chem. Sci.*, 2024, **15**, 18715-18750.
23. G. Decher, *Science*, 1997, **277**, 1232-1237.
24. M. H. Iqbal, H. Kerdjoudj and F. Boulmedais, *Chem. Sci.*, 2024, **15**, 9408-9437.
25. S. Horike, *Bull. Chem. Soc. Jpn.*, 2023, **96**, 887-898.
26. T. Kitao, *Bull. Chem. Soc. Jpn.*, 2024, **97**, uoae103.
27. D. Jiang, X. Xu, Y. Bando, S. M. Alshehri, M. Eguchi, T. Asahi and Y. Yamauchi, *Bull. Chem. Soc. Jpn.*, 2024, **97**, uoae074.
28. K. Wang, X. Qiao, H. Ren, Y. Chen and Z. Zhang, *J. Am. Chem. Soc.*, 2025, **147**, 8063-8082.
29. M. Eguchi, A. S. Nugraha, A. E. Rowan, J. Shapter and Y. Yamauchi, *Adv. Sci.*, 2021, **8**, 2100539.
30. N. Shioya, T. Mori, K. Ariga and T. Hasegawa, *Japanese Journal of Applied Physics*, 2024, **63**, 060102.
31. J. Kim, J. H. Kim and K. Ariga, *Joule*, 2017, **1**, 739-768.
32. P. Wang, W. Tao, T. Zhou, J. Wang, C. Zhao, G. Zhou and Y. Yamauchi, *Adv. Mater.*, 2024, **36**, 2404418.
33. D. Barreca and C. Maccato, *CrystEngComm*, 2023, **25**, 3968-3987.
34. A. Jancik-Prochazkova and K. Ariga, *Research*, 2025, **8**, 0624.
35. A. Javed, N. Kong, M. Mathesh, W. Duan and W. Yang, *Sci. Technol. Adv. Mater.*, 2024, **25**, 2345041.
36. S. Yu, N. S. Rejinold, G. Choi and J.-H. Choy, *Nanoscale Horiz.*, 2025, **10**, 460-483.
37. A. B. Grommet, M. Feller and R. Klajn, *Nat. Nanotechnol.*, 2020, **15**, 256-271.
38. J. Wordsworth, T. M. Benedetti, S. V. Somerville, W. Schuhmann, R. D. Tilley and J. J. Gooding, *Angew. Chem., Int. Ed.*, 2022, **61**, e202200755.
39. L. Gura, E. A. Soares, J. Paier, F. Stavale and H. J. Freund, *Top. Catal.*, 2023, **66**, 1073-1086.
40. S.-M. Lu, K. J. Vannoy, J. E. Dick and Y.-T. Long, *J. Am. Chem. Soc.*, 2023, **145**, 25043-25055.
41. Y. Ma, H. Li, J. Liu and D. Zhao, *Nat. Chem. Rev.*, 2024, **8**, 915-931.
42. K. Liu, R. Epszstein, S. Lin, J. Qu and M. Sun, *ACS Nano*, 2024, **18**, 21633-21650.
43. J. Zhou, M. Zhang, Y. Lin, J. Xu, C. Pan, Y. Lou, Y. Zhang, Y. Wang, Y. Dong, Y. Zhu, J. Zhang and Z. Lin, *Nano Energy*, 2024, **125**, 109529.
44. K. Ariga, *Micromachines*, 2024, **15**, 282.
45. A. C. Aragonès, N. L. Haworth, N. Darwish, S. Ciampi, E. J. Mannix, G. G. Wallace, I. Diez-Perez and M. L. Coote, *Nature*, 2016, **531**, 88-91.
46. K. Adachi, S. Fa, K. Wada, K. Kato, S. Ohtani, Y. Nagata, S. Akine and T. Ogoshi, *J. Am. Chem. Soc.*, 2023, **145**, 8114-8121.
47. H. Takezawa, Y. Fujii, T. Murase and M. Fujita, *Angew. Chem., Int. Ed.*, 2022, **61**, e202203970.
48. H. Wang, X. Liu, Y. Wang, Y. Tian, Y. Huang, D. Huang and X. Liu, *Environ. Sci. Nano*, 2024, **11**, 1978-1984.
49. A. Botos, J. Biskupek, T. W. Chamberlain, G. A. Rance, C. T. Stoppiello, J. Sloan, Z. Liu, K. Suenaga, U. Kaiser and A. N. Khlobystov, *J. Am. Chem. Soc.*, 2016, **138**, 8175-8183.
50. Z. Li, X. Zhang, H. Cheng, J. Liu, M. Shao, M. Wei, D. G. Evans, H. Zhang and X. Duan, *Adv. Energy Mater.*, 2020, **10**, 1900486.
51. J. Fu, S. Pang, Y. Zhang, X. Li, B. Song, D. Peng, X. Zhang and L. Jiang, *Adv. Sci.*, 2024, **11**, 2308388.
52. X. Zhang, L. Cheng, Y. Lu, J. Tang, Q. Lv, X. Chen, Y. Chen and J. Liu, *Nano-Micro Lett.*, 2022, **14**, 1-21.
53. R. Liang, Y. Li, M. Huo, H. Lin and Y. Chen, *ACS Appl. Mater. Interfaces*, 2019, **11**, 42917-42931.
54. X. Lian, Y.-P. Chen, T.-F. Liu and H.-C. Zhou, *Chem. Sci.*, 2016, **7**, 6969-6973.
55. X. Lian, Y. Huang, Y. Zhu, Y. Fang, R. Zhao, E. Joseph, J. Li, J. P. Pellois and H. C. Zhou, *Angew. Chem., Int. Ed.*, 2018, **57**, 5725-5730.
56. G. Llauroadé - Capdevila, A. Veciana, M. A. Guarducci, A. Mayoral, R. Pons, L. Hertle, H. Ye, M. Mao, S. Sevim and D. Rodríguez - San - Miguel, *Adv. Mater.*, 2024, **36**, 2306345.
57. J. H. Lee, W. Bonte, S. Corthals, F. Krumeich, M. Ruitenbeek and J. A. van Bokhoven, *Ind. Eng. Chem. Res.*, 2019, **58**, 5140-5145.
58. S. Acharya, D. D. Sarma, Y. Golan, S. Sengupta and K. Ariga, *J. Am. Chem. Soc.*, 2009, **131**, 11282-11283.
59. V. Oskoei, M. Mathesh and W. Yang, *Chem.--Eur. J.*, 2024, **30**, e202401256.
60. J. Liu, T. A. Goetjen, Q. Wang, J. G. Knapp, M. C. Wasson, Y. Yang, Z. H. Syed, M. Delferro, J. M. Notestein and O. K. Farha, *Chem. Soc. Rev.*, 2022, **51**, 1045-1097.
61. Z. Chen, F. Hu, Z. Lin, J. Hu, R. Shen, Y. Lin and X. Y. Liu, *Small Science*, 2021, **1**, 2000049.
62. O. Rifaie-Graham, J. Yeow, A. Najer, R. Wang, R. Sun, K. Zhou, T. N. Dell, C. Adrianus, C. Thanapongpibul and M. Chami, *Nat. Chem.*, 2023, **15**, 110-118.
63. X. Liu, Y. Hao, R. Popovtzer, L. Feng and Z. Liu, *Adv. Healthc. Mater.*, 2021, **10**, 2001167.
64. M. Kuepfert, E. Ahmed and M. Weck, *Macromolecules*, 2021, **54**, 3845-3853.
65. X. Yao, X. Cao, J. He, L. Hao, H. Chen, X. Li and W. Huang, *Small*, 2024, **20**, 2405816.
66. T. Lorenzetto, D. Frigatti, F. Fabris and A. Scarso, *Adv. Synth. Catal.*, 2022, **364**, 1776-1797.
67. P. Liu, G. Chen and J. Zhang, *Molecules*, 2022, **27**, 1372.
68. V. Mouarrawis, R. Plessius, J. I. Van der Vlugt and J. N. Reek, *Front. Chem.*, 2018, **6**, 623.
69. Q. Guan, Y. Fang, X. Wu, R. Ou, X. Zhang, H. Xie, M. Tang and G. Zeng, *Mater. Today*, 2023, **64**, 138-164.

70. L. Chen and Q. Xu, *Matter*, 2019, **1**, 57-89.
71. K. Ariga, *Materials*, 2025, **18**, 654.
72. K. Ariga, *Nanoscale Horiz.*, 2021, **6**, 364-378.
73. K. Ariga, Y. Lvov and G. Decher, *Phys. Chem. Chem. Phys.*, 2022, **24**, 4097-4115.
74. H. Chen, C. Jia, X. Zhu, C. Yang, X. Guo and J. F. Stoddart, *Nat. Rev. Mater.*, 2023, **8**, 165-185.
75. C. Gao, Q. Gao, C. Zhao, Y. Huo, Z. Zhang, J. Yang, C. Jia and X. Guo, *Natl. Sci. Rev.*, 2024, **11**, nwae236.
76. Y. Zhang, P. Song, Q. Fu, M. Ruan and W. Xu, *Nat. Commun.*, 2014, **5**, 4238.
77. B. Shen, H. Wang, H. Xiong, X. Chen, E. G. T. Bosch, I. Lazić, W. Qian and F. Wei, *Nature*, 2022, **607**, 703-707.
78. M. B. Steffensen, D. Rotem and H. Bayley, *Nat. Chem.*, 2014, **6**, 603-607.
79. C.-Y. Li, S. Duan, J. Yi, C. Wang, P. M. Radjenovic, Z.-Q. Tian and J.-F. Li, *Sci. Adv.*, 2020, **6**, eaba6012.
80. D. M. Eigler and E. K. Schweizer, *Nature*, 1990, **344**, 524-526.
81. Y. Sugimoto, K. Miki, M. Abe and S. Morita, *Phys. Rev. B*, 2008, **78**, 205305.
82. S.-W. Hla, L. Bartels, G. Meyer and K.-H. Rieder, *Phys. Rev. Lett.*, 2000, **85**, 2777-2780.
83. L. Gross, F. Mohn, N. Moll, P. Liljeroth and G. Meyer, *Science*, 2009, **325**, 1110-1114.
84. J. Guan, C. Jia, Y. Li, Z. Liu, J. Wang, Z. Yang, C. Gu, D. Su, K. N. Houk, D. Zhang and X. Guo, *Sci. Adv.*, 2018, **4**, eaar2177.
85. S. Sato, T. Yamasaki and H. Isobe, *Proc. Natl. Acad. Sci.*, 2014, **111**, 8374-8379.
86. T. Iwamoto, Y. Watanabe, T. Sadahiro, T. Haino and S. Yamago, *Angew. Chem., Int. Ed.*, 2011, **50**, 8342-8344.
87. T. Matsuno and H. Isobe, *Bull. Chem. Soc. Jpn.*, 2023, **96**, 406-419.
88. Y. Ji, H. Yang and W. Yan, *Catalysts*, 2017, **7**, 367.
89. P. Del Campo, C. Martínez and A. Corma, *Chem. Soc. Rev.*, 2021, **50**, 8511-8595.
90. T.-Y. Zhou, B. Auer, S. J. Lee and S. G. Telfer, *J. Am. Chem. Soc.*, 2019, **141**, 1577-1582.
91. X. Liu, F. Pang, M. He and J. Ge, *Nano Res.*, 2017, **10**, 3638-3647.
92. C. Tang, H.-S. Wang, H.-F. Wang, Q. Zhang, G.-L. Tian, J.-Q. Nie and F. Wei, *Adv. Mater.*, 2015, **27**, 4516-4522.
93. J. Zhang, J. Liu, L. Xi, Y. Yu, N. Chen, S. Sun, W. Wang, K. M. Lange and B. Zhang, *J. Am. Chem. Soc.*, 2018, **140**, 3876-3879.
94. W. Zhu, Z. Chen, Y. Pan, R. Dai, Y. Wu, Z. Zhuang, D. Wang, Q. Peng, C. Chen and Y. Li, *Adv. Mater.*, 2019, **31**, 1800426.
95. L. Qin, J. Gan, D. Niu, Y. Cao, X. Duan, X. Qin, H. Zhang, Z. Jiang, Y. Jiang, S. Dai, Y. Li and J. Shi, *Nat. Commun.*, 2022, **13**, 91.
96. L.-F. Gutiérrez, S. Hamoudi and K. Belkacemi, *Catalysts*, 2011, **1**, 97-154.
97. H. Chen, K. Shen, Q. Mao, J. Chen and Y. Li, *ACS Catal.*, 2018, **8**, 1417-1426.
98. J. K. Nørskov, T. Bligaard, J. Rossmeisl and C. H. Christensen, *Nat. Chem.*, 2009, **1**, 37-46.
99. K. Ariga, *Nanoscale*, 2022, **14**, 10610-10629.
100. W. Chaikittisilp, Y. Yamauchi and K. Ariga, *Adv. Mater.*, 2022, **34**, 2107212.
101. X. Huang, H. Mutlu and P. Théato, *Colloid Polym. Sci.*, 2021, **299**, 325-341.
102. W. Li, Q. Yue, Y. Deng and D. Zhao, *Adv. Mater.*, 2013, **25**, 5129-5152.
103. L. Wang, U. S. Schubert and S. Hoeppeener, *Chem. Soc. Rev.*, 2021, **50**, 6507-6540.
104. S. Casalini, C. A. Bortolotti, F. Leonardi and F. Biscarini, *Chem. Soc. Rev.*, 2017, **46**, 40-71.
105. M. Ishii, Y. Yamashita, S. Watanabe, K. Ariga and J. Takeya, *Nature*, 2023, **622**, 285-291.
106. A. M. Tokmachev, D. V. Averyanov, I. A. Karateev, I. S. Sokolov, O. E. Parfenov and V. G. Storchak, *Adv. Funct. Mater.*, 2020, **30**, 2002691.
107. S. Roy, X. Zhang, A. B. Puthirath, A. Meiyazhagan, S. Bhattacharyya, M. M. Rahman, G. Babu, S. Susarla, S. K. Saju and M. K. Tran, *Adv. Mater.*, 2021, **33**, 2101589.
108. S. In Yoon, H. Park, Y. Lee, C. Guo, Y. J. Kim, J. S. Lee, S. Son, M. Choe, D. Han, K. Kwon, J. Lee, K. Y. Ma, A. Ghassami, S. W. Moon, S.-Y. Park, B. K. Kang, Y.-J. Kim, S. Koo, A. Genco, J. Shim, A. Tartakovsky, Y. Duan, F. Ding, S. Ahn, S. Ryu, J.-Y. Kim, W. S. Yang, M. Chhowalla, Y. S. Park, S. K. Min, Z. Lee and H. S. Shin, *Sci. Adv.*, 2024, **10**, eadp9804.
109. M. J. Prieto, H. W. Klemm, F. Xiong, D. M. Gottlob, D. Menzel, T. Schmidt and H.-J. Freund, *Angew. Chem., Int. Ed.*, 2018, **57**, 8749-8753.
110. M. J. Prieto, T. Mullan, M. Schlutow, D. M. Gottlob, L. C. Tănase, D. Menzel, J. Sauer, D. Usvyat, T. Schmidt and H.-J. Freund, *J. Am. Chem. Soc.*, 2021, **143**, 8780-8790.
111. J. Wang, W. Liu, G. Luo, Z. Li, C. Zhao, H. Zhang, M. Zhu, Q. Xu, X. Wang, C. Zhao, Y. Qu, Z. Yang, T. Yao, Y. Li, Y. Lin, Y. Wu and Y. Li, *Energy Environ. Sci.*, 2018, **11**, 3375-3379.
112. C. Jia, Q. Wang, J. Yang, K. Ye, X. Li, W. Zhong, H. Shen, E. Sharman, Y. Luo and J. Jiang, *ACS Catal.*, 2022, **12**, 3420-3429.
113. C.-C. Hou, H.-F. Wang, C. Li and Q. Xu, *Energy Environ. Sci.*, 2020, **13**, 1658-1693.
114. Y. Chen, J. Lin, Q. Pan, X. Liu, T. Ma and X. Wang, *Angew. Chem.*, 2023, **135**, e202306469.
115. F. Lin, M. Xu, K. K. Ramasamy, Z. Li, J. L. Klinger, J. A. Schaidle and H. Wang, *ACS Catal.*, 2022, **12**, 13555-13599.
116. Q. Zhang, S. Gao and J. Yu, *Chem. Rev.*, 2022, **123**, 6039-6106.
117. D. Yao, Y. Wang, Y. Li, Y. Zhao, J. Lv and X. Ma, *ACS Catal.*, 2018, **8**, 1218-1226.
118. D. Munoz-Santiburcio and D. Marx, *Chem. Rev.*, 2021, **121**, 6293-6320.
119. J. Shen, G. Liu, Y. Han and W. Jin, *Nat. Rev. Mater.*, 2021, **6**, 294-312.
120. K. Guan, Y. Guo, Z. Li, Y. Jia, Q. Shen, K. Nakagawa, T. Yoshioka, G. Liu, W. Jin and H. Matsuyama, *Nat. Commun.*, 2023, **14**, 1016.
121. X. Zhang, G. Li, G. Chen, D. Wu, Y. Wu and T. D. James, *Adv. Funct. Mater.*, 2021, **31**, 2106139.
122. Z. Wang, Y. Hou, G. Tang, Y. Li, Y. Zhao, Y. Yu, G. Wang, X. Yan and K. Fan, *Fundamental Research*, 2024, DOI: doi.org/10.1016/j.fmre.2024.11.013.
123. C. Keum, C.-M. Hirschbiegel, S. Chakraborty, S. Jin, Y. Jeong and V. M. Rotello, *Nano Conver.*, 2023, **10**, 42.
124. M. S. Kim, J. Lee, H. S. Kim, A. Cho, K. H. Shim, T. N. Le, S. S. A. An, J. W. Han, M. I. Kim and J. Lee, *Adv. Funct. Mater.*, 2020, **30**, 1905410.
125. L. Jiao, H. Yan, Y. Wu, W. Gu, C. Zhu, D. Du and Y. Lin, *Angew. Chem., Int. Ed.*, 2020, **59**, 2565-2576.



126. J. Xi, R. Zhang, L. Wang, W. Xu, Q. Liang, J. Li, J. Jiang, Y. Yang, X. Yan, K. Fan and L. Gao, *Adv. Funct. Mater.*, 2021, **31**, 2007130.
127. I. Nath, J. Chakraborty and F. Verpoort, *Chem. Soc. Rev.*, 2016, **45**, 4127-4170.
128. M. Zhao, S. Ou and C.-D. Wu, *Acc. Chem. Res.*, 2014, **47**, 1199-1207.
129. J. Gaitzsch, X. Huang and B. Voit, *Chem. Rev.*, 2016, **116**, 1053-1093.
130. J. Li, Y. Anraku and K. Kataoka, *Angew. Chem., Int. Ed.*, 2020, **59**, 13526-13530.
131. F. Cuomo, A. Ceglie, A. De Leonardis and F. Lopez, *Catalysts*, 2018, **9**, 1.
132. P. Wen, A. Dirisala, H. Guo, X. Liu, S. Kobayashi, H. Kinoh, T. Anada, M. Tanaka, K. Kataoka and J. Li, *Journal of Controlled Release*, 2025, **382**, 113683.
133. Q. Shi, Z. Yong, M. H. Uddin, R. Fu, D. Sikdar, L. W. Yap, B. Fan, Y. Liu, D. Dong and W. Cheng, *Adv. Mater.*, 2022, **34**, 2105630.
134. J. Vapaavuori, C. G. Bazuin and A. Priimagi, *J. Mater. Chem. C*, 2018, **6**, 2168-2188.
135. P. B. Rathod, K. A. Kumar, K. Yakkala, M. P. Singh, A. A. Athawale and A. K. Pandey, *Next Nanotechnol.*, 2025, **8**, 100148.
136. S. Hooshmand, S. M. Hayat, A. Ghorbani, M. Khatami, K. Pakravanan and M. Darroudi, *Curr. Med. Chem.*, 2021, **28**, 777-799.
137. K. Ariga, *Respon. Mat.*, 2024, **2**, e20240011.
138. I. Ortiz-Rivera, M. Mathesh and D. A. Wilson, *Acc. Chem. Res.*, 2018, **51**, 1891-1900.
139. M. Mathesh, E. Bhattarai and W. Yang, *Angew. Chem.*, 2022, **134**, e202113801.
140. Q. Xu, Y. Tao, Z. Wang, H. Zeng, J. Yang, Y. Li, S. Zhao, P. Tang, J. Zhang and M. Yan, *Adv. Mater.*, 2024, **36**, 2311624.
141. G. Kang, S. Hu, C. Guo, R. Arul, S. M. Sibug-Torres and J. J. Baumberg, *Nat. Commun.*, 2024, **15**, 9220.
142. X. Li, X. Yang, J. Zhang, Y. Huang and B. Liu, *ACS Catal.*, 2019, **9**, 2521-2531.
143. Y. Liu, X. Su, J. Ding, J. Zhou, Z. Liu, X. Wei, H. B. Yang and B. Liu, *Chem. Soc. Rev.*, 2024, **53**, 11850-11887.
144. J. I. J. Choi, T.-S. Kim, D. Kim, S. W. Lee and J. Y. Park, *ACS Nano*, 2020, **14**, 16392-16413.
145. A. Kolmakov and D. W. Goodman, *Rev. Sci. Instrum.*, 2003, **74**, 2444-2450.
146. M. Rößler, P. Geng and J. Wintterlin, *Rev. Sci. Instrum.*, 2005, **76**.
147. R. Toyoshima, M. Yoshida, Y. Monya, Y. Kousa, K. Suzuki, H. Abe, B. S. Mun, K. Mase, K. Amemiya and H. Kondoh, *J. Phys. Chem. C*, 2012, **116**, 18691-18697.
148. F. J. Giessibl, S. Hembacher, H. Bielefeldt and J. Mannhart, *Science*, 2000, **289**, 422-425.
149. J. Il Jake Choi, L. K. Ono, H. Cho, K.-J. Kim, H.-B. Kang, Y. Qi and J. Y. Park, *ACS Nano*, 2023, **17**, 25679-25688.
150. L. Zhang, D.-M. Tang and C. Liu, *Small*, 2024, **20**, 2405736.
151. J. Dai, Y. Sun, Z. Liu, Y. Zhang, S. Duan and R. Wang, *Angew. Chem.*, 2024, **136**, e202409673.
152. Y. Wang, L. Qiu, L. Zhang, D.-M. Tang, R. Ma, C.-L. Ren, F. Ding, C. Liu and H.-M. Cheng, *Sci. Adv.*, 2022, **8**, eabo5686.
153. B. Baumgartner, A. Wach, X. Ye, E. Ploetz and B. M. Weckhuysen, *Adv. Mater.*, 2025, **n/a**, e2415135.
154. B. de Nijs, F. Benz, S. J. Barrow, D. O. Sigle, R. Chikkaraddy, A. Palma, C. Carnegie, M. Kamp, R. Sundararaman, P. Narang, O. A. Scherman and J. J. Baumberg, *Nat. Commun.*, 2017, **8**, 994.
155. H. Zhang, C. Wang, H.-L. Sun, G. Fu, S. Chen, Y.-J. Zhang, B.-H. Chen, J. R. Anema, Z.-L. Yang, J.-F. Li and Z.-Q. Tian, *Nat. Commun.*, 2017, **8**, 15447.
156. Ö. Karahan, E. Biçer, A. Taşdemir, A. Yürüm and S. A. Gürsel, *Eur. J. Inorg. Chem.*, 2018, **2018**, 1073-1079.
157. M. Lv, X. Wu, W. Wang, D. Han, S. Chen, Y. Hu, Q. Zhang, Q. Wang and R. Wei, *ACS Sensors*, 2025, DOI: 10.1021/acssensors.4c02391.
158. H. Woo, A. M. Devlin and A. J. Matzger, *J. Am. Chem. Soc.*, 2023, **145**, 18634-18641.
159. Y. Zhao, W. Liu, J. Zhao, Y. Wang, J. Zheng, J. Liu, W. Hong and Z.-Q. Tian, *Int. J. Extreme Manuf.*, 2022, **4**, 022003.
160. T. Hartman, C. S. Wondergem, N. Kumar, A. van den Berg and B. M. Weckhuysen, *J. Phys. Chem. Lett.*, 2016, **7**, 1570-1584.
161. J.-H. Tian, B. Liu, Li, Z.-L. Yang, B. Ren, S.-T. Wu, Tao and Z.-Q. Tian, *J. Am. Chem. Soc.*, 2006, **128**, 14748-14749.
162. H. Bi, C.-A. Palma, Y. Gong, P. Hasch, M. Elbing, M. Mayor, J. Reichert and J. V. Barth, *J. Am. Chem. Soc.*, 2018, **140**, 4835-4840.
163. S. R. V. Parambil, S. Karmakar, F. A. Rahimi and T. K. Maji, *ACS Appl. Mater. Interfaces*, 2023, **15**, 27821-27831.
164. C. Sun, L. Yang, M. A. Ortuño, A. M. Wright, T. Chen, A. R. Head, N. López and M. Dincă, *Angew. Chem., Int. Ed.*, 2021, **60**, 7845-7850.
165. B. Dong, N. Mansour, T.-X. Huang, W. Huang and N. Fang, *Chem. Soc. Rev.*, 2021, **50**, 6483-6506.
166. D. Chen, Y. Cheng, N. Zhou, P. Chen, Y. Wang, K. Li, S. Huo, P. Cheng, P. Peng, R. Zhang, L. Wang, H. Liu, Y. Liu and R. Ruan, *J. Clean. Prod.*, 2020, **268**, 121725.
167. X. Li, T. Wan, J. Qiu, H. Wei, F. Qin, Y. Wang, Y. Liao, Z. Huang and X. Tan, *Appl. Catal. B Environ.*, 2017, **217**, 591-602.
168. K. Liu, X. Qiao, C. Huang, X. Li, Z. Xue and T. Wang, *Angew. Chem., Int. Ed.*, 2021, **60**, 14365-14369.
169. P. Lohner, M. Zmyslija, J. Thurn, J. K. Pape, R. Gerasimaitė, J. Keller - Findeisen, S. Groer, B. Deuringer, R. Süß and A. Walther, *Angew. Chem.*, 2021, **133**, 24028-24034.
170. M. Jaugstetter, N. Blanc, M. Kratz and K. Tschulik, *Chem. Soc. Rev.*, 2022, **51**, 2491-2543.
171. Y. Men, Y. Tan, P. Li, Y. Jiang, L. Li, X. Su, X. Men, X. Sun, S. Chen and W. Luo, *Angew. Chem.*, 2024, **136**, e202411341.
172. H. Ren and M. A. Edwards, *Curr. Opin. Electroche.*, 2021, **25**, 100632.
173. L. Zhang, O. J. Wahab, A. A. Jallow, Z. J. O'Dell, T. Pungsrisai, S. Sridhar, K. L. Vernon, K. A. Willets and L. A. Baker, *Anal. Chem.*, 2024, **96**, 8036-8055.
174. S.-M. Lu, M.-Y. Li and Y.-T. Long, *J. Phys. Chem. Lett.*, 2022, **13**, 4653-4659.
175. Y. Liu, X. Li, J. Chen and C. Yuan, *Front. Chem.*, 2020, **8**, 573865.
176. C.-H. Chen, E. R. Ravenhill, D. Momotenko, Y.-R. Kim, S. C. S. Lai and P. R. Unwin, *Langmuir*, 2015, **31**, 11932-11942.
177. M. Huang, L. Yu, M. Zhang, Z. Wang, B. Xiao, Y. Liu, J. He and S. Chang, *Small*, 2021, **17**, 2101911.
178. A. P. Ivanov, E. Instuli, C. M. McGilvery, G. Baldwin, D. W. McComb, T. Albrecht and J. B. Edel, *Nano Lett.*, 2011, **11**, 279-285.
179. W. Pan, R. You, S. Zhang, Y. Chang, F. Zhou, Q. Li, X. Chen, X. Duan and Z. Han, *Anal. Chim. Acta*, 2023, **1251**, 341035.

180. T. Dadosh, Y. Gordin, R. Krahne, I. Khivrich, D. Mahalu, V. Frydman, J. Sperling, A. Yacoby and I. Bar-Joseph, *Nature*, 2005, **436**, 677-680.
181. Y. Qing, H. Tamagaki-Asahina, S. A. Ionescu, M. D. Liu and H. Bayley, *Nat. Nanotechnol.*, 2019, **14**, 1135-1142.
182. T. J. Anderson and B. Zhang, *Acc. Chem. Res.*, 2016, **49**, 2625-2631.
183. N. Kong, J. He and W. Yang, *J. Phys. Chem. Lett.*, 2023, **14**, 8513-8524.
184. Z. Sun, Z. Gu and W. Ma, *Anal. Chem.*, 2023, **95**, 3613-3620.
185. L. Chen, E. E. Tanner, C. Lin and R. G. Compton, *Chem. Sci.*, 2018, **9**, 152-159.
186. L.-X. Wang, M. Zhang, C. Sun, L.-X. Yin, B. Kang, J.-J. Xu and H.-Y. Chen, *Angew. Chem., Int. Ed.*, 2022, **61**, e202117177.
187. N. Kong, J. Guo, S. Chang, J. Pan, J. Wang, J. Zhou, J. Liu, H. Zhou, F. M. Pfeffer, J. Liu, C. J. Barrow, J. He and W. Yang, *J. Am. Chem. Soc.*, 2021, **143**, 9781-9790.
188. B. Li, X. Huang, Y. Lu, Z. Fan, B. Li, D. Jiang, N. Sojic and B. Liu, *Adv. Sci.*, 2022, **9**, 2204715.
189. Y. Lu, X. Huang, S. Wang, B. Li and B. Liu, *ACS Nano*, 2023, **17**, 3809-3817.
190. J. Kim, C. Renault, N. Nioradze, N. Arroyo-Currás, K. C. Leonard and A. J. Bard, *J. Am. Chem. Soc.*, 2016, **138**, 8560-8568.
191. C. L. Bentley, M. Kang and P. R. Unwin, *J. Am. Chem. Soc.*, 2017, **139**, 16813-16821.
192. C.-C. Chen, Y. Zhou and L. A. Baker, *Annu. Rev. Anal. Chem.*, 2012, **5**, 207-228.
193. C. Dette, M. R. Hurst, J. Deng, M. R. Nellist and S. W. Boettcher, *ACS Appl. Mater. Interfaces*, 2018, **11**, 5590-5594.
194. D. Freitas, X. Chen, H. Cheng, A. Davis, B. Fallon and X. Yan, *ChemPlusChem*, 2021, **86**, 434-445.
195. F. Blanc, M. Leskes and C. P. Grey, *Acc. Chem. Res.*, 2013, **46**, 1952-1963.
196. S. Yuan, Q. Qian, Y. Zhou, S. Zhao, L. Lin, P. Duan, X. Xu, J. Shi, W. Xu, A. Feng, J. Shi, Y. Yang and W. Hong, *Small*, 2022, **18**, 2104554.
197. K. Ge, H. Shao, Z. Lin, P.-L. Taberna and P. Simon, *Nat. Nanotechnol.*, 2024, **20**, 196-208.
198. M. J. Van Vleet, T. Weng, X. Li and J. Schmidt, *Chem. Rev.*, 2018, **118**, 3681-3721.
199. T. Chen, F. Wang, S. Cao, Y. Bai, S. Zheng, W. Li, S. Zhang, S. X. Hu and H. Pang, *Adv. Mater.*, 2022, **34**, 2201779.
200. H. Feng, C. Li and H. Shan, *Appl. Clay Sci.*, 2009, **42**, 439-445.
201. S. Bordiga, F. Bonino, K. P. Lillerud and C. Lamberti, *Chem. Soc. Rev.*, 2010, **39**, 4885-4927.
202. Y. Zhu, J. Wang, H. Chu, Y.-C. Chu and H. M. Chen, *ACS Energy Lett.*, 2020, **5**, 1281-1291.
203. W. Cheng, H. Su and Q. Liu, *Acc. Chem. Res.*, 2022, **55**, 1949-1959.
204. H. Su, W. Zhou, H. Zhang, W. Zhou, X. Zhao, Y. Li, M. Liu, W. Cheng and Q. Liu, *J. Am. Chem. Soc.*, 2020, **142**, 12306-12313.
205. H. Pan, K. Liu, A. Caracciolo and P. Casavecchia, *Chem. Soc. Rev.*, 2017, **46**, 7517-7547.
206. L. Ploenes, P. Straňák, H. Gao, J. Küpper and S. Willitsch, *Mol. Phys.*, 2021, **119**, e1965234.